

## Rational Design of 4-Aryl-1,2,3-Triazoles for Indoleamine 2,3-Dioxygenase 1 Inhibition

Ute F. Röhrig,<sup>†,‡,#</sup> Somi Reddy Majjigapu,<sup>†,§,#</sup> Aurélien Grosdidier,<sup>‡</sup> Sylvian Bron,<sup>‡,||</sup> Vincent Stroobant,<sup>⊥</sup> Luc Pilotte,<sup>⊥</sup> Didier Colau,<sup>⊥</sup> Pierre Vogel,<sup>§,†</sup> Benoît J. Van den Eynde,<sup>⊥</sup> Vincent Zoete,<sup>\*,‡</sup> and Olivier Michielin<sup>||,\*,†,‡</sup>

<sup>†</sup>Ludwig Center for Cancer Research of the University of Lausanne, CH-1015 Lausanne, Switzerland

<sup>‡</sup>Swiss Institute of Bioinformatics, Molecular Modeling Group, CH-1015 Lausanne, Switzerland

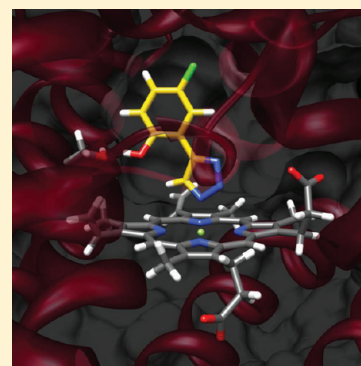
<sup>§</sup>Laboratory of Glycochemistry and Asymmetric Synthesis, Ecole Polytechnique Fédérale de Lausanne (EPFL), CH-1015 Lausanne, Switzerland

<sup>||</sup>Pluridisciplinary Centre for Clinical Oncology (CePO), Centre Hospitalier Universitaire Vaudois (CHUV), Lausanne, Switzerland

<sup>⊥</sup>Ludwig Institute for Cancer Research, Brussels Branch, and de Duve Institute, Université Catholique de Louvain, B-1200 Brussels, Belgium

### **S** Supporting Information

**ABSTRACT:** Indoleamine 2,3-dioxygenase 1 (IDO1) is an important therapeutic target for the treatment of diseases such as cancer that involve pathological immune escape. Starting from the scaffold of our previously discovered IDO1 inhibitor 4-phenyl-1,2,3-triazole, we used computational structure-based methods to design more potent ligands. This approach yielded highly efficient low molecular weight inhibitors, the most active being of nanomolar potency both in an enzymatic and in a cellular assay, while showing no cellular toxicity and a high selectivity for IDO1 over tryptophan 2,3-dioxygenase (TDO). A quantitative structure–activity relationship based on the electrostatic ligand–protein interactions in the docked binding modes and on the quantum chemically derived charges of the triazole ring demonstrated a good explanatory power for the observed activities.



### ■ INTRODUCTION

Many tumors develop the capacity to actively suppress a potentially effective immune response.<sup>1</sup> The enzyme indoleamine 2,3-dioxygenase 1 (IDO1, EC 1.13.11.52) is one of the key players in this pathological immune escape and has therefore been selected as a therapeutic target for pharmacological interventions.<sup>2–4</sup> IDO1 catalyzes the initial and rate-limiting step in the catabolism of tryptophan (Trp) along the kynurenine pathway.<sup>5,6</sup> By depleting Trp and accumulating Trp catabolites, IDO1 exerts a local immunosuppressive effect on T-lymphocytes.<sup>7–10</sup> The observations that many human tumors constitutively express IDO1<sup>11</sup> and that increased IDO1 expression in tumor cells is correlated with poor prognosis for survival in several cancer types<sup>12</sup> led to the hypothesis that its inhibition might enhance the efficacy of cancer treatments. Indeed, results from *in vitro* and *in vivo* studies have suggested that the efficacy of therapeutic vaccination or chemotherapy may be improved by concomitant administration of an IDO1 inhibitor.<sup>11,13–16</sup> Very recently, it has been shown that the functionally related enzyme tryptophan 2,3-dioxygenase (TDO) may be a complementary anticancer target.<sup>17,18</sup>

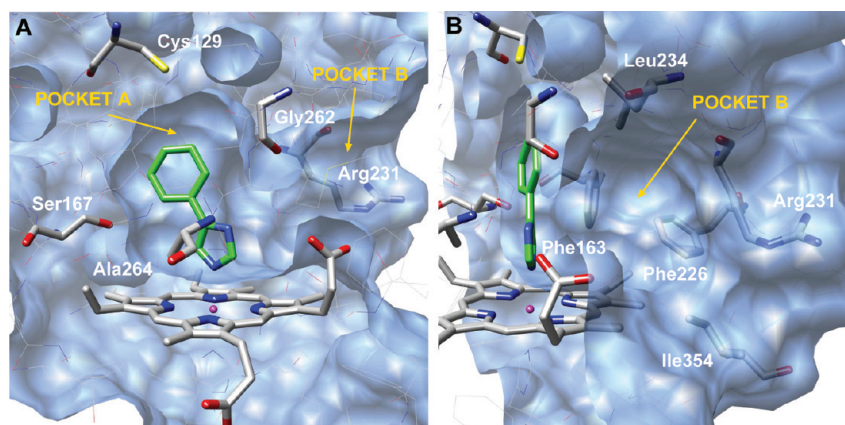
The IDO1-like protein Indoleamine 2,3-dioxygenase 2 (IDO2)<sup>19,20</sup> shares 44% of sequence homology with IDO1. However, its physiological role remains unclear due to (i) very

low Trp degradation activity, (ii) the presence of polymorphisms abolishing its enzymatic activity in about 50% of Caucasians, and (iii) the presence of multiple splice variants.<sup>21–23</sup>

IDO1 is an extrahepatic heme-containing enzyme that displays less substrate specificity than TDO.<sup>6</sup> In the first step of the catalytic cycle, IDO1 binds both the substrate and molecular oxygen in the distal heme site. The enzyme catalyzes the cleavage of the pyrrole ring of the substrate and incorporates both oxygen atoms before releasing *N*-formyl kynurenine, which is subsequently hydrolyzed to kynurenine by a cytosolic formamidase.<sup>24</sup> The two available crystal structures of IDO1 include the heme-bound ligands cyanide and 4-phenylimidazole (PIM), respectively.<sup>25</sup> Mutant analyses showed that none of the polar amino acid residues in the distal heme site are essential for the activity of the enzyme, suggesting a reaction mechanism involving only the substrate and the dioxygen molecule.<sup>25–27</sup> In the active form of IDO1, the heme iron is in its ferrous state (Fe<sup>2+</sup>), while in its inactive form, the heme iron is in the ferric (Fe<sup>3+</sup>) state. Formally, the catalytic cycle of IDO1 does not alter the oxidation state of the

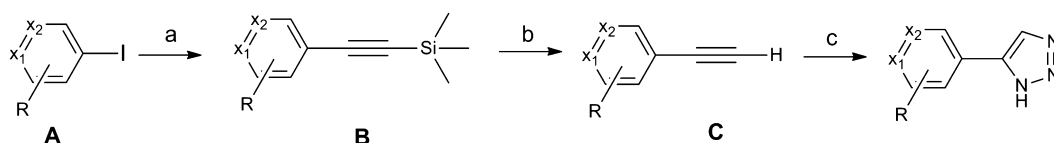
Received: February 24, 2012

Published: May 22, 2012



**Figure 1.** X-ray structure of IDO1: binding site with PIM ligand (green). (A) Two hydrophobic pockets and residues in hydrogen-bonding distance are labeled. (B) Side view, highlighting the residues that form pocket B.

### Scheme 1<sup>a</sup>



<sup>a</sup>Reagents, conditions, and yields: (a) TMSA, PdCl<sub>2</sub>(PPh<sub>3</sub>)<sub>2</sub>, Et<sub>3</sub>N, CuI, dioxane, 45 °C, 5 h, up to 95%; (b) KF, MeOH, rt, 3 h, up to 85%; (c) TMSN<sub>3</sub>, CuI, DMF/MeOH (9:1), 100 °C, 10–12 h, 30–83%,

heme, but as IDO1 is prone to autoxidation, a reductant is necessary in the enzymatic assay to maintain enzyme activity. Cytochrome b5 has been suggested to be responsible for IDO1 reduction in vivo.<sup>28–30</sup>

The two crystal structures of human IDO1<sup>25</sup> open the way for the in silico design of new IDO1 inhibitors. In the PIM-bound X-ray structure (PDB accession code 2D0T), the ligand is bound in a deep binding site with its phenyl ring inside a hydrophobic pocket (pocket A, Figure 1) and one imidazole nitrogen coordinated to the heme iron at a distance of 2.1 Å. The PIM binding site consists of residues Tyr126, Cys129, Val130, Phe163, Phe164, Ser167, Leu234, Gly262, Ser263, Ala264, and the heme ring. Possible hydrogen-bonding sites are the hydroxyl group of Ser167, the CO group of Gly262, the NH group of Ala264, and the heme 7-propionate group. Ligands larger than PIM may also interact with Phe226, Arg231, Ser235, Phe291, Ile354, and Leu384, which are located at the binding site entrance. Here, additional hydrogen bonds are possible with the side chain of Arg231. A hydrophobic pocket in this region is provided by Phe163, Phe226, Arg231, Leu234, Ile354, and the heme ring (pocket B, Figure 1). The cyanide-bound structure (2D0U) differs from the PIM-bound structure mainly in the access to pocket A, which is hindered by an inward-movement of the backbone of loop 262–266 and the side chain of Phe163, suggesting some flexibility in the active site. In both structures, two buffer molecules (*N*-cyclohexyltaurine) are bound at the entrance of the active site, hydrogen-bonding to the heme propionate and interacting with pocket B.

The oldest known IDO1 inhibitors with activities in the micromolar range are Trp derivatives and  $\beta$ -carbolines.<sup>6,13,31–36</sup> In recent years, many redox-active IDO1 inhibitors with IC<sub>50</sub> values of up to 60 nM have been discovered.<sup>37–44</sup> However, there exists the possibility that these act through interference with the chemical reducing agents in the enzymatic assay

(methylene blue and ascorbate) rather than through IDO1-specific interactions.<sup>30</sup> Other classes of inhibitors derived from a target-based screen of the NCI diversity set,<sup>45</sup> the 4-phenylimidazole scaffold,<sup>46</sup> the indole scaffold,<sup>47,48</sup> the *S*-benzylisothiourea scaffold,<sup>49</sup> a high throughput screen,<sup>23</sup> and a virtual screen<sup>50</sup> have been described. The most potent and promising compounds known today are the competitive hydroxyamidine inhibitors developed by Incyte,<sup>15,51,52</sup> with enzymatic IC<sub>50</sub> values of about 60 nM. Compound INCB24360, whose structure has not been disclosed yet, is currently undergoing a phase I clinical trial.

We have previously described a number of new IDO1 inhibitors based on a structure-based in silico design strategy.<sup>53</sup> Among the new scaffolds, we discovered 4-phenyl-1,2,3-triazole (1) to inhibit IDO1 with an IC<sub>50</sub> value of 60  $\mu$ M. Some modifications of this scaffold have very recently been described by another group,<sup>54</sup> but improvement of the IC<sub>50</sub> value was limited to less than a factor of 2 compared to the parent compound. The aim of the present work was to rationally optimize the 4-phenyl-1,2,3-triazole scaffold relying on our in-house drug design tools.<sup>55–61</sup> Substituted 1,2,3-triazoles have been found to be useful drug scaffolds<sup>62–66</sup> and are synthetically accessible under mild conditions through copper(I)-catalyzed azide–alkyne cycloaddition.<sup>67–69</sup>

Here, we computationally designed new ligands and docked them into the IDO1 active site using EADock-DSS<sup>55–59</sup> and AttractingCavities<sup>70</sup> in combination with the parameters derived from SwissParam<sup>60</sup> and a Morse-like metal binding potential (MMBP).<sup>61</sup> Candidates that displayed a good filling of the A pocket and favorable heme interactions were selected for synthesis and tested in an enzymatic assay for IDO1 inhibition. Bioisosteres of the 4-phenyl-1,2,3-triazole scaffold were also investigated. Active ligands were subsequently tested in cellular assays on murine and on human IDO1. Counter-screening against TDO determined their selectivity for IDO1.

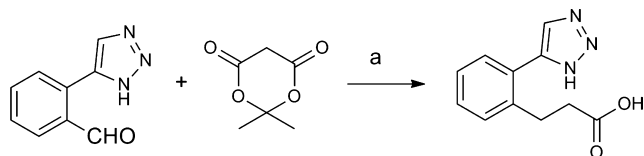
To rationalize the observed activities, we then developed a quantitative structure–activity relationship (QSAR) based on the docking results and on quantum chemical calculations.

Following this strategy, we obtained 39 triazole-based IDO1 inhibitors, the most potent having an IC<sub>50</sub> value in the nanomolar range both in the enzymatic and in the cellular assays while being inactive on TDO and showing no detectable toxicity on the cellular level.

## CHEMISTRY

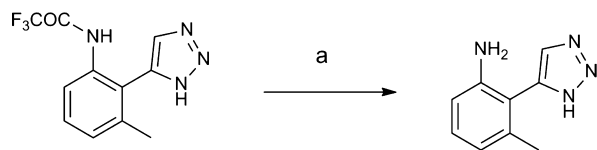
The 4-phenyl-1,2,3-triazole derivatives were synthesized using existing protocols or procedures adapted from the literature. The N-unsubstituted 1,2,3-triazoles (**1–42**, **62–64**, and **74**) were synthesized according to the method developed by Yamamoto and co-workers,<sup>71</sup> which involves reaction of ethynyl derivatives with trimethylsilyl azide (Scheme 1). The ethynyl derivatives were synthesized from iodo substrates by the Sonogashira coupling reaction.<sup>72</sup> Compound **33** was synthesized by treatment of **74** with 6 N HCl at room temperature.<sup>73</sup> Compound **34** was derived from compound **30** by treatment with Meldrum's acid in TEAF at 95–100 °C (Scheme 2).<sup>74</sup> Deprotection of the trifluoroacetamide of **41**

### Scheme 2<sup>a</sup>



<sup>a</sup>Reagents, conditions, and yields: (a) TEAF, 95–100 °C, 3 h, 45%.

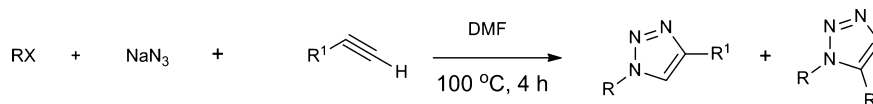
### Scheme 3<sup>a</sup>



<sup>a</sup>Reagents, conditions, and yields: (a) N<sub>2</sub>H<sub>4</sub>·H<sub>2</sub>O, dioxane, reflux, 2.5 h, 50%.

with N<sub>2</sub>H<sub>4</sub>·H<sub>2</sub>O provided **40** (Scheme 3).<sup>75</sup> All other compounds were synthesized according to literature procedures [**58**,<sup>76</sup> **61**,<sup>77</sup> (**54**, **55**, **56**, and **57**, Scheme 4),<sup>78,79</sup> (**43**, **44**, **45**, **46**, and **47**, Scheme 5),<sup>80,81</sup> (**48**, **49**, and **50**, Scheme 6),<sup>82–84</sup> (**51**, **52**, and **53**, Scheme 6),<sup>82,85,86</sup> and (**59** and **60**, Scheme 7)<sup>82</sup>] or were commercially available (compounds **65–73**).

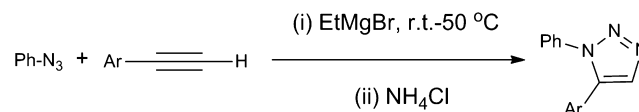
### Scheme 4



(i) R = benzyl chloride, R<sup>1</sup> = Ph

(ii) R = *n*-butyl iodide, R<sup>1</sup> = Ph

### Scheme 5



Ar = Ph, 4F-Ph, 3Me-Ph, 3Cl-Ph, 2-OMe-Ph, 3-Pyridyl

## RESULTS AND DISCUSSION

**Compounds with Aryl Substitutions.** Docking PIM into the IDO1 active site using a Morse-like metal binding potential (MMBP),<sup>61</sup> we observe an excellent agreement with the X-ray structure<sup>25</sup> (rmsd 0.3 Å) and an iron–nitrogen bond of 2.1 Å.<sup>53</sup>

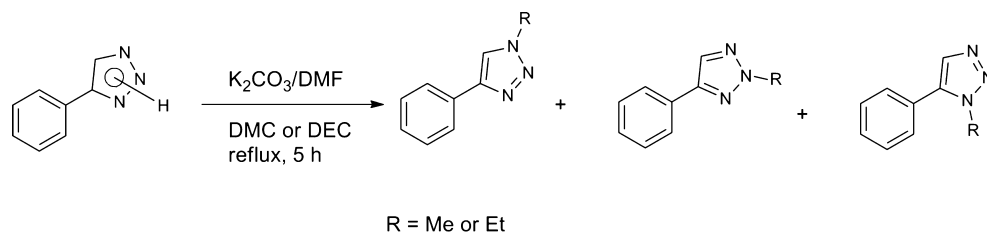
Our previously published triazoles<sup>53</sup> (Table 1, compounds **1**, **2**, and **3**) are structurally similar to PIM, with the imidazole ring replaced by a triazole ring. The docked structure of the parent compound **1** closely resembles that of PIM, with one of the nitrogen atoms coordinated to the heme iron (Figure 2A–D). As the triazole ring can occur in three different tautomers (Figure 2A–C) and in a deprotonated form (Figure 2D), we docked all four isomers into the IDO1 active site. Because the MMBP parameters are the same for all nitrogen atoms with a free electron pair,<sup>61</sup> the MMBP cannot distinguish between the binding energies of the deprotonated form and the neutral triazole tautomers. All isomers show similar binding modes (BM) with a conserved position of the phenyl ring, the only difference being the orientation of the triazole ring. In the following, we therefore show only the BM of the deprotonated forms of the N-unsubstituted triazoles.

The *meta*-pyridyl compound (**3**) is more than an order of magnitude less active than the phenyl compound (**1**), while the *para*-pyridyl compound (**2**) retains the activity of **1**. The docked BM of the three compounds do not directly explain this difference in activity, as the pyridyl nitrogen is not making any obvious interaction with the protein (Figure 2E,F).

In the following, we tested different derivatives of **1** with substitutions in *para*, *meta*, and *ortho* positions and combinations of these (Table 1, Figure 2G–O). All substitutions in *para* position of the phenyl ring of the 4-phenyl-1,2,3-triazole scaffold (**1**) reduce the IDO1 inhibitory activity (Table 1, compounds **4**, **5**, **6**, and **7**). The fact that the reduction in activity is correlated with the size of the substituent ( $F < Cl < CH_3 < CF_3$ ) as well as results from docking suggest that the protein binding pocket is rather tight in this region and does not provide space for additional groups (Figure 2G).

Substitutions in the *meta* position generally increase the ligand's activity on IDO1, in agreement with the docking results, which show the filling of a small subpocket in this position (Figure 2H,I). Generally, electron-withdrawing and hydrophobic substitutions yield better inhibitors. The only *meta*-substituted compounds with a lower activity than

Scheme 6



Scheme 7

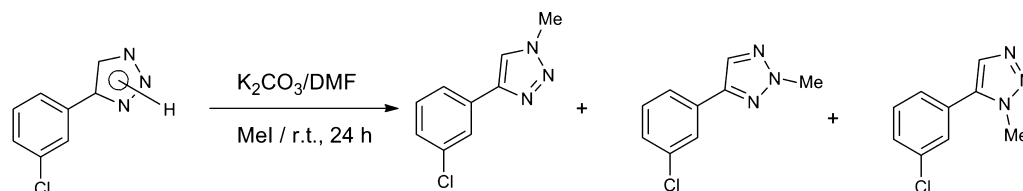


Table 1. Phenyl-Ring Substituted Derivatives

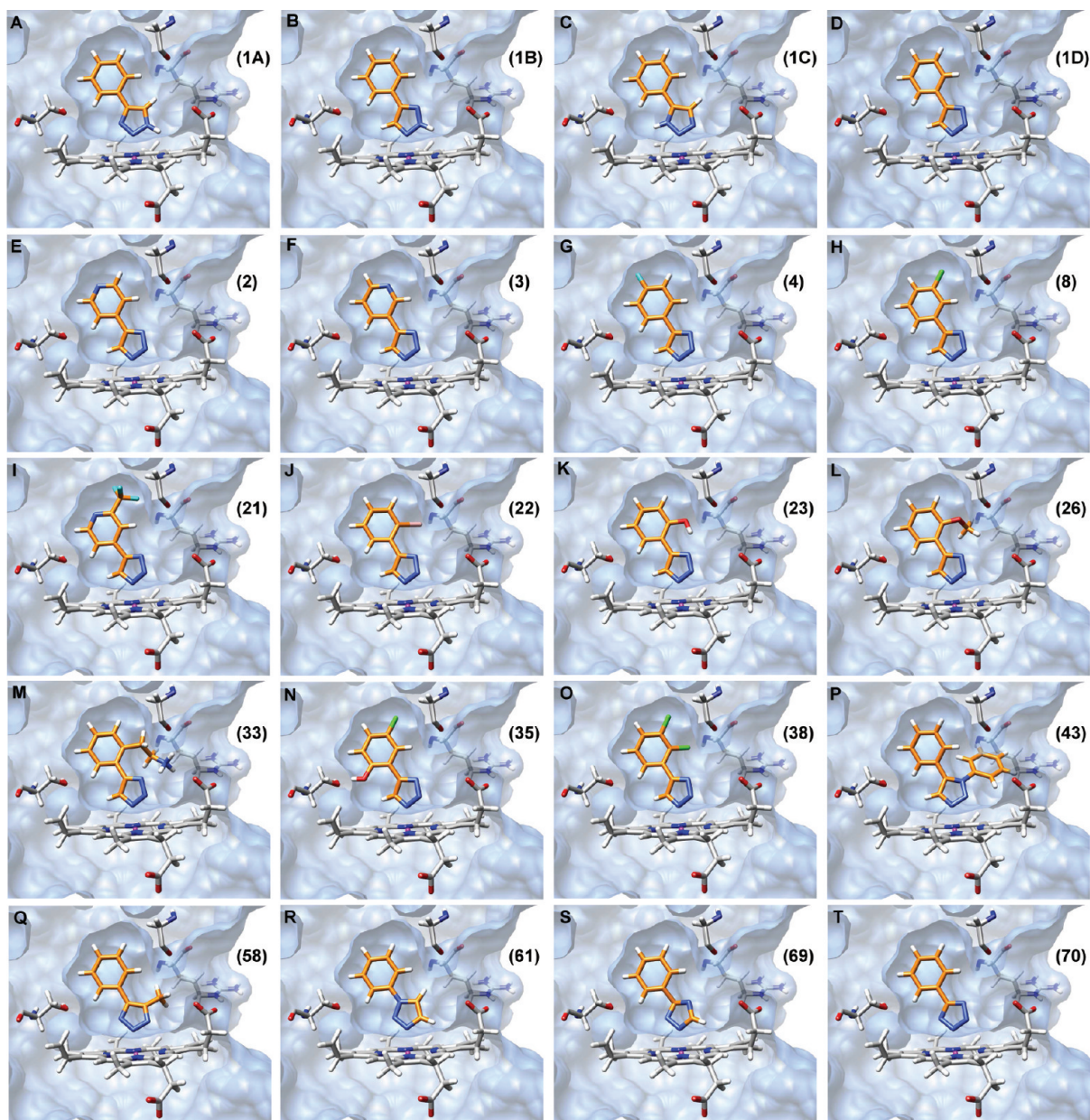
	X <sub>1</sub>	X <sub>2</sub>	R	IC <sub>50</sub> [μM] <sup>a</sup>		X <sub>1</sub>	X <sub>2</sub>	R	IC <sub>50</sub> [μM] <sup>a</sup>
1	C	C		83	22	C	C	2-Br	6.4
2	N	C		85	23	C	C	2-OH	15
3	C	N		1000	24	C	C	2-Cl	32
4	C	C	4-F	190	25	C	C	2-CH <sub>3</sub>	39
5	C	C	4-Cl	530	26	C	C	2-NH <sub>2</sub>	60
6	C	C	4-CH <sub>3</sub>	1000	27	C	C	2-F	80
7	C	C	4-CF <sub>3</sub>	2300	28	C	C	2-C <sub>2</sub> H <sub>5</sub>	230
8	C	C	3-Cl	1.2	29	C	C	2-CF <sub>3</sub>	650
9	C	C	3-Br	2.0	30	C	C	2-CHO	1300
10	C	C	3-CN	2.8	31	C	C	2-NHCH <sub>3</sub>	1800
11	C	C	3-CF <sub>3</sub>	6.0	32	C	C	2-OCH <sub>3</sub>	NI
12	C	C	3-C <sub>2</sub> H <sub>5</sub>	13	33	C	C	2-CH <sub>2</sub> CH <sub>2</sub> NH <sub>2</sub>	NI
13	C	C	3-NO <sub>2</sub>	15	34	C	C	2-CH <sub>2</sub> CH <sub>2</sub> COOH	NI
14	C	C	3-CH <sub>3</sub>	22	35	C	C	2-OH,5-Cl	0.33 <sup>b</sup>
15	C	C	3-F	47	36	C	C	2-CH <sub>3</sub> ,5-Cl	4.3
16	C	C	3-OH	310	37	C	C	2,5-di-Cl	6.4
17	C	C	3-NH <sub>2</sub>	1500	38	C	C	2,3-di-Cl	23
18	N	C	3-Cl	2.8	39	C	C	2-CH <sub>3</sub> ,3-Cl	72
19	N	C	3-Br	3.3	40	C	C	2-NH <sub>2</sub> ,6-CH <sub>3</sub>	1200
20	N	C	3-F	7.4	41	C	C	2-NHCOCF <sub>3</sub> ,6-CH <sub>3</sub>	3000
21	N	C	3-CF <sub>3</sub>	15	42	C	C	2-CH <sub>3</sub> ,5-NH <sub>2</sub>	3200

<sup>a</sup>IC<sub>50</sub> values are the mean of at least two independent assays. <sup>b</sup>IC<sub>50</sub> value of 0.071 μM at pH 7.4.

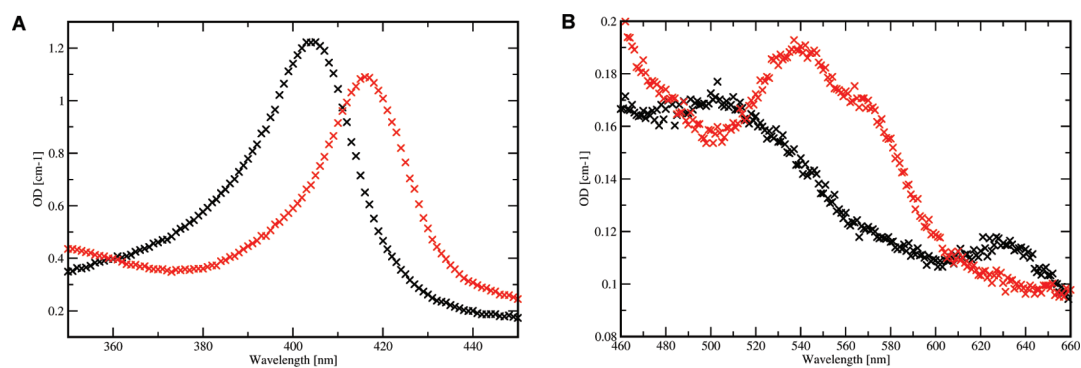
compound **1** are the ones with the hydrophilic hydroxyl (**16**, IC<sub>50</sub> = 310 μM) and amino (**17**, 1500 μM) substitutions. Combination of a favorable *meta* substitution with the *para*-pyridyl substitution (**2**) improves the activity only in the case of the fluoro substitution, the least active compound (**20**), while the activities of the other compounds (**18**, **19**, and **21**) remain approximately constant.

Compounds substituted in the *ortho* position show a wide variability of their IC<sub>50</sub> values, ranging from 6.4 μM to no detectable activity. Apparently, large substituents are not allowed in the *ortho* position, even though docking results

suggest that these could extend to pocket B (Figure 2M). Hydroxyl (**23**, IC<sub>50</sub> = 15 μM) and amino (**26**, 60 μM) substitutions in the *ortho* position are much better tolerated than in the *meta* position, and they even lead to increased activity. This could be due to (i) better solvation, (ii) an intramolecular hydrogen bond formed between N3 of the triazole and the *o*-OH or *o*-NH<sub>2</sub> group (Figure 2K), or (iii) an intermolecular hydrogen bond formed between the ligand and Ser167. While the last hypothesis has been proposed for the *o*-OH-substituted 4-phenylimidazole analogue<sup>46</sup> and could also explain the inactivity of the *o*-methoxyl substituted ligand (**32**),



**Figure 2.** Proposed binding modes from docking results. The compound numbers are given in parentheses. Carbon atoms are shown in orange/gray, nitrogen in blue, oxygen in red, bromine in pink, chlorine in green, fluorine in cyan, iron in magenta, and hydrogen in white.



**Figure 3.** UV spectra of ferric IDO1 without (black) and with 1 mM concentration of compound 35 (red). In the presence of 35, the Soret peak (A) shifts from 404 to 416 nm and the Q-bands (B) from 499 and 633 nm to 538 and 566 nm, demonstrating a direct binding of the ligand to the heme iron.

it is in discrepancy with the docked BM of compounds **23** and **26** (Figure 2K,L).

When testing doubly substituted compounds, we noted that the substitution effects are not additive. Four of these compounds, all featuring a *meta*-chloro substituent, showed a better activity than the parent compound (**1**). The 2,5-disubstituted compounds (**36** and **37**) were more potent than the corresponding 2,3-disubstituted compounds (**38** and **39**), which is probably due to steric constraints in the IDO1 binding pocket. Docking results favor the 2,3-disubstituted compounds (Figure 2O), as the 2,5-disubstituted compounds (**36** and **37**) fail to bind to the heme, highlighting the lack of binding site flexibility in our model. The only compound displaying a lower IC<sub>50</sub> value than the *meta*-chloro substitution alone (**8**, 1.2 μM) is the 2-OH,5-Cl substituted compound (**35**, 330 nM, Figure 2N). Again, the *ortho*-hydroxyl substitution leads to an especially favorable activity.

Kinetic experiments with IDO1 inhibitors often yield uncompetitive or noncompetitive modes of inhibition even when there exists strong evidence, as in the case of PIM,<sup>25,32</sup> that they bind directly in the active site and should therefore be competitive with respect to the substrate L-Trp.<sup>32,46,48,54,87</sup> However, the interpretation of IDO1 inhibition kinetics may be complicated by the preferential binding of some inhibitors to the inactive ferric form of IDO1 and by the presence of a second substrate, dioxygen. To obtain a more direct indication of the binding site of our triazole compounds, we measured UV spectra of ferric IDO1 with and without compound **35** (Figure 3). The absorption spectrum of substrate-free ferric IDO1 exhibits a Soret peak at 404 nm and Q-bands at 499 and 633 nm (plus a shoulder at 533 nm) as described in the literature.<sup>88</sup> In presence of compound **35**, the Soret peak strongly shifts to 416 nm together with a hypochromic effect, while the Q-bands shift to 538 and 570 nm. This change in optical absorption is similar to the changes induced by the binding of PIM (peaks at 412.5, 533, and 560 nm) and of pyridine (peaks at 419, 538, and 570 nm) to IDO1, both of which have been confirmed to bind directly to the heme iron.<sup>25,32</sup>

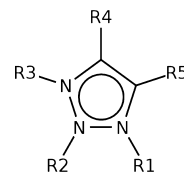
**Compounds with Substituted Triazole Rings.** Besides the parent compound 4-phenyl-1,2,3-triazole (**1**), we docked its isomer 1-phenyl-1,2,3-triazole (**61**) in the IDO1 active site (Figure 2R) and observed a close similarity to PIM and compound **1**, as all three compounds are sterically almost identical and provide a nitrogen atom with a free electron pair for heme binding. However, **61** does not show any inhibitory activity on IDO1 in the enzymatic assay (Table 2).

Additionally, we observed that any substitution of the triazole ring in position R1, R2, R3, or R5 in combination with the phenyl substitution in position R4 also completely abolished activity (Table 2). This is a significant difference to the imidazole analogues, where, for example, 1-benzyl-5-phenyl-imidazole is more active than PIM.<sup>46</sup> Taking these results together, they hint at the necessity of an ionizable NH group in the triazoles and at the hypothesis that the active form of the triazole for IDO1 inhibition could be its deprotonated, anionic form.

The inactivity of the 4,5-disubstituted compound **58** (Figure 2Q), which preserves the ionizable NH group of the triazole ring, could be related to its increased pK<sub>a</sub> value (9.11 vs 8.62 for **1**, Table 4), due to the electron-donating substitution on the triazole ring, or it could be due to steric effects.

**Compounds with Modified Scaffolds.** Any attempt to replace the 1,2,3-triazole scaffold by bioisosteres such as 1,2,4-

Table 2. Triazole-Ring Substituted Derivatives



	R1	R2	R3	R4	R5	IC <sub>50</sub> [μM] <sup>a</sup>
<b>1</b>	H			phenyl	H	83
<b>43</b>			phenyl	phenyl	H	NI
<b>44</b>			phenyl	4-F-phenyl	H	NI
<b>45</b>			phenyl	3-CH <sub>3</sub> -phenyl	H	NI
<b>46</b>			phenyl	3-Cl-phenyl	H	NI
<b>47</b>			phenyl	2-OCH <sub>3</sub> -phenyl	H	NI
<b>48</b>			methyl	phenyl	H	NI
<b>49</b>	methyl			phenyl	H	NI
<b>50</b>		methyl		phenyl	H	NI
<b>51</b>			ethyl	phenyl	H	NI
<b>52</b>		ethyl		phenyl	H	NI
<b>53</b>	ethyl			phenyl	H	NI
<b>54</b>			<i>n</i> -butyl	phenyl	H	NI
<b>55</b>	<i>n</i> -butyl			phenyl	H	NI
<b>56</b>			benzyl	phenyl	H	NI
<b>57</b>	benzyl			phenyl	H	NI
<b>58</b>	H			phenyl	methyl	NI
<b>59</b>			methyl	3-Cl-phenyl	H	NI
<b>60</b>	methyl			3-Cl-phenyl	H	NI
<b>61</b>	phenyl			H	H	NI

<sup>a</sup>IC<sub>50</sub> values are the mean of at least two independent assays.

triazole (**69**), tetrazole (**70**), isoxazole (**71**), pyridine (**72**), or pyrimidine (**73**) completely abolished IDO1 inhibitory activity (Table 3). Also compounds with linkers between the aromatic moieties (**62** and **63**), a cyclohexene analogue (**64**), and benzotriazoles (**65** and **66**) failed to show any activity.

Steric reasons may play a role for some of these compounds. For example, docking results for compounds **63** (filled volume of pocket A: 85%) and **65** (78%) show that these do not fill the IDO1 binding pocket as tightly as the other compounds (**1**: 96%). Compounds with two aromatic six-membered rings (**72** and **73**) apparently need an iron-binding nitrogen in 3-position, as only 3-phenylpyridine has been shown to be active on IDO1 (IC<sub>50</sub> = 161 μM).<sup>46</sup>

Other compounds (**69**, **70**, and **71**), however, are sterically so similar to compound **1** that their inactivity on IDO1 must be due to electronic effects. Compound **69** (Figure 2S) is a closely related isomer of compound **1**, however, with a higher pK<sub>a</sub> value (9.29 vs 8.62), which may prevent its deprotonation under experimental conditions. In contrast, the tetrazole (**70**, Figure 2T) has a very low pK<sub>a</sub> value (4.53) and should therefore be deprotonated under experimental conditions. However, quantum chemical atomic point charges show that its electron density is mainly concentrated on N1 and N4 (charge -0.36), which are next to the phenyl ring, while N2 and N3, which are available for heme iron binding, only carry small negative charges (-0.17). In active compounds, the negative charge on the iron-binding nitrogen atom ranges from -0.33 to -0.46. Similarly to compound **70**, in the inactive isoxazole **71**, the nitrogen atom available for iron binding is

Table 3. Modified Scaffolds

	Structure	IC <sub>50</sub> [ $\mu$ M] <sup>a</sup>
62		NI
63		NI
64		NI
65		NI
66		NI
67		1800
68		NI
69		NI
70		NI
71		NI
72		NI
73		NI

<sup>a</sup>IC<sub>50</sub> values are the mean of at least two independent assays.

very poor in electrons (charge  $-0.12$ ) due to the electro-negative neighboring oxygen atom.

**pK<sub>a</sub> Measurements.** To better understand the electronic properties of the triazoles, we carried out pK<sub>a</sub> measurements of selected compounds (Table 4). The parent compound (**1**) has a pK<sub>a</sub> value of 8.62 for deprotonation of its triazole ring, 0.64 pK<sub>a</sub> units more acidic than the unsubstituted 1,2,3-triazole (9.26).<sup>89</sup> Compounds with electron-withdrawing substituents on the phenyl ring are more acidic than **1**, because these substituents stabilize the negative charge on the triazole.

In Figure 4A, we plot the measured pK<sub>a</sub> values as a function of the Hammett substituent constants  $\sigma$ ,<sup>90</sup> assuming (i) that the influence of substituents is additive,  $\sigma = \sigma_{ortho} + \sigma_{meta} + \sigma_{para}$  which is a common assumption,<sup>90</sup> and (ii) that the influence of a substituent is equal in *ortho* and in *para* position,  $\sigma_{ortho} = \sigma_{para}$  which should be valid if steric hindrance is low and if no special interactions arise in *ortho* position.

For all compounds with *meta* and *para* substitutions (black stars in Figure 4A), a very good linear relationship is obtained:

$$pK_a = 8.607 - 0.787 \times \sigma \quad (1)$$

with a correlation coefficient of 0.997. Compounds with a chloro substituent in *ortho* position (**24**, **37**, and **38**) follow this correlation quite closely, but compounds with an oxygen-containing substituent in *ortho* position (**24**, **37**, and **38**) are clear outliers of this relationship.

The *ortho*-methoxyl substituent of **32** leads to a more basic pK<sub>a</sub> value than predicted from its  $\sigma$  value, suggesting a hydrogen bond between the neutral triazole and the substituent that renders deprotonation of the triazole less favorable. The

opposite is observed for compounds **23** and **35** featuring an *ortho*-hydroxyl substitution, which display more acidic pK<sub>a</sub> values than predicted from their  $\sigma$  value, suggesting that here a hydrogen bond between the substituent and the anionic triazole stabilizes the negatively charged form of the triazole. This interpretation is further supported by the strong shift of one pK<sub>a</sub> unit from 9.95 to 10.95 for the phenolic pK<sub>a</sub> of compound **23**, as this hydrogen now serves to stabilize the monoanion.

All measured pK<sub>a</sub> values are higher than the pH at which the enzymatic assay is carried out (6.5). However, the pK<sub>a</sub> of a ligand in water does not necessarily reflect its pK<sub>a</sub> in the protein-bound state. It has been shown, e.g., that thiols binding to CYP450-CAM show a pK<sub>a</sub> shift of 4 units as compared to their values in water.<sup>91</sup> It is therefore possible that the triazoles bind to IDO1 in their deprotonated form. Taking into consideration the inactivity of all triazole compounds lacking an ionizable NH group (Table 2) or having a high pK<sub>a</sub> value, this hypothesis becomes the most likely scenario.

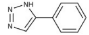
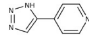
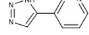
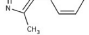
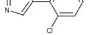
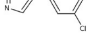
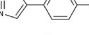
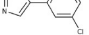
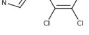
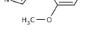
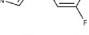



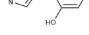
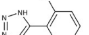
We have further tested this hypothesis by carrying out an enzymatic assay at pH 7.4 instead of pH 6.5 for compound **35**. As expected, **35** shows a higher activity (IC<sub>50</sub> = 71 nM) at pH 7.4 than at pH 6.5 (IC<sub>50</sub> = 330 nM, see Figure S2 in the Supporting Information).

**Quantitative Structure–Activity Relationship.** Early on during our efforts to optimize the potency of the triazole ligands, we noticed a correlation between the activities of the *meta*-substituted compounds and the Hammett  $\sigma$  constants ( $r = 0.62$ ), a correlation that could be even improved by adding the hydrophobicity constant  $\pi$  as a second parameter ( $r = 0.90$ , Figure 4B).<sup>90</sup> In this model, the more electron-withdrawing and the more hydrophobic the substituent on the phenyl ring, the better the potency of the triazole compound against IDO1. The influence of the hydrophobicity is not surprising, as docking suggests that the substituent in *meta* position will be placed inside a hydrophobic subpocket of the IDO1 active site (Figure 2H–J). The electronic properties of the substituent, however, control the electronic properties of the triazole ring, as exemplified by our pK<sub>a</sub> measurements. Two possible interpretations of the correlation between IDO1 inhibitory activity and  $\sigma$  are therefore that (i) IDO1 inhibition of the triazoles increases with decreasing electron density on the triazole ring, possibly influencing the heme binding strength (heme-binding strength hypothesis), or (ii) IDO1 inhibition increases with decreasing pK<sub>a</sub> of the triazole ring, because the ligand must be deprotonated in order to be active (deprotonation hypothesis). A combination of both effects is possible.

We investigated this question by quantum chemical calculations. The direct calculation of binding energies of the triazole compounds to a heme model system is a complex task due to the existence of six possible ligand–heme orientations of the three tautomeric forms and the deprotonated form of the ligands, which, in combination with two possible iron redox states (ferric and ferrous form), leads to 12 different binding energies. Therefore, the complete set of calculations was only carried out for the parent compound **1**, from which favorable ligand–heme orientations were obtained (details given in Supporting Information).

Taking solvation effects into account by a polarizable continuum model (PCM),<sup>92</sup> the neutral parent compound (**1**) binds more strongly to ferric heme ( $-4.5$  kcal/mol, 3H tautomer binding with N1 to iron) than to ferrous heme ( $-0.3$

Table 4. pK<sub>a</sub> Values and Hammett  $\sigma$  Values

Compound	pK <sub>a</sub> as Base	pK <sub>a</sub> as Acid <sup>a</sup>	$\sigma$ <sup>b</sup>
Imidazole <sup>89</sup>	6.95	14.52	
4-Phenylimidazole (PIM) <sup>89</sup>	6.10	13.42	
1,2,3-Triazole <sup>89</sup>	1.17	9.26	
4-Phenyl-1,2,3-triazole ( <b>1</b> ) <sup>133</sup>	0.40	<sup>c</sup>	
Benzotriazole ( <b>65</b> ) <sup>131</sup>	1.60	8.60	
1,2,4-Triazole <sup>89</sup>	2.19	10.26	
3-Phenyl-1,2,4-triazole ( <b>69</b> ) <sup>89</sup>	2.05	9.29	
Tetrazole <sup>89</sup>		4.79	
5-Phenyltetrazole ( <b>70</b> ) <sup>89</sup>		4.53	
Pyridine <sup>135</sup>	5.23		
Phenol <sup>135</sup>		9.99	
 ( <b>1</b> )		8.62 (0.02)	0.00
 ( <b>2</b> )		7.85 (0.01)	0.94
 ( <b>3</b> )		8.14 (0.01)	0.55
 ( <b>58</b> )		9.11 (0.01)	
 ( <b>24</b> )		8.50 (0.01)	0.23
 ( <b>8</b> )		8.32 (0.01)	0.37
 ( <b>5</b> )		8.46 (0.01)	0.23
 ( <b>37</b> )		8.17 (0.03)	0.60
 ( <b>38</b> )		8.06 (0.01)	0.60
 ( <b>32</b> )		8.99 (0.02)	-0.27
 ( <b>15</b> )		8.38 (0.01)	0.34
 ( <b>20</b> )		7.59 (0.01)	1.28
 ( <b>18</b> )		7.60 (0.01)	1.31
 ( <b>16</b> )		8.46 (0.01, triazole)	0.12
		10.13 (0.02, phenol)	
 ( <b>23</b> )		8.58 (0.02, triazole)	-0.37
		10.95 (0.03, phenol)	
 ( <b>35</b> )		8.25 (0.01, triazole)	0.00
		10.56 (0.04, phenol)	

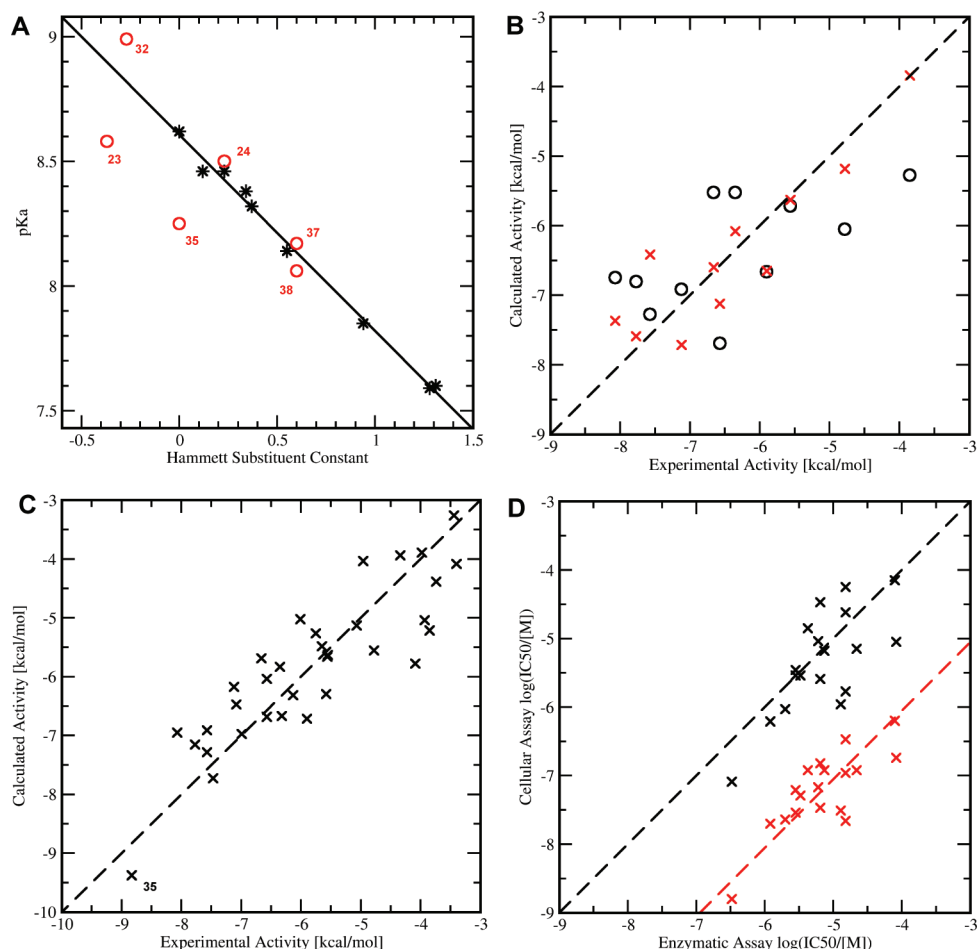
<sup>a</sup>Standard deviation given in parentheses. <sup>b</sup>The definition of the Hammett  $\sigma$  values is given in the text. <sup>c</sup>The acidic pK<sub>a</sub> value of 6.32 given in refs 89,134 goes back to a reference dating from the beginning of the 20th century and is obviously wrong.

kcal/mol, 2H tautomer binding with N1 to iron). These binding energies are significantly lower than the binding energies of the deprotonated form of **1** to both ferric (−17.0 kcal/mol, binding with N1 to iron) and to ferrous (−1.4 kcal/mol, binding with N1 to iron) heme. The neutral form of compound **8**, which has an electron-withdrawing *meta*-chloro substituent on the phenyl ring, binds even more weakly to ferric heme (−3.7 kcal/mol) and just as weakly to ferrous heme

(−0.4 kcal/mol) than the parent compound. Its deprotonated form shows similar binding energies for ferric heme (−16.7 kcal/mol) and for ferrous heme (−1.6 kcal/mol) as compound **1**.

In summary, quantum chemical calculations suggest that heme binding strength does not increase with decreasing electron density on the triazole ring but that the deprotonated form of the triazoles binds much more strongly to heme than





**Figure 4.** (A) Correlation between the Hammett substituent constant and the measured  $pK_a$  values, assuming (i) that the influence of substituents is additive, and (ii) that the influence of a substituent is equal in *ortho* and in *para* position. Compounds without a substitution in *ortho* position are shown as black stars, and the black line is a linear fit to these points ( $r = 0.997$ ). (B) Correlation between experimental and calculated activities of *meta*-substituted compounds using the Hammett substituent constant alone (black,  $r = 0.62$ ) or in combination with the hydrophobicity parameter (red,  $r = 0.90$ ). The black dotted line denotes a perfect correlation. (C) QSAR relationship using the quantum chemical triazole charges and the electrostatic interaction/solvation term from the docking as descriptors (see text). (D) Correlation between the  $IC_{50}$  values measured in the enzymatic assay and the  $IC_{50}$  values measured in the cellular assays on hIDO1 (black) and on mIDO1 (red).

the neutral form. They support thus the deprotonation hypothesis.

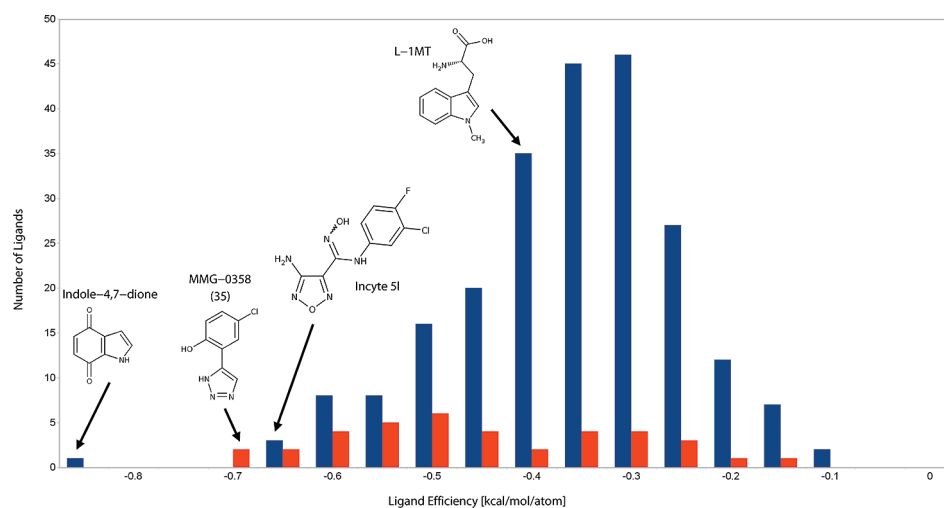
In the following, we developed a quantitative structure–activity relationship (QSAR) for the triazole compounds based on our docking results. All standard terms such as electrostatic interactions, van der Waals interactions, and solvation terms are calculated based on the CHARMM22 classical force field<sup>93,94</sup> and the FACTS implicit solvent model<sup>95</sup> (see Experimental Section). However, this procedure does not include the electronic effects described above. We therefore decided to include an additional electronic term in the QSAR model. As the Hammett constants are only available for a subset of our compounds, we replaced them by an electronic parameter that could be determined for all compounds using quantum chemical calculations. After many trials, we chose to use the sum of atomic charges on the deprotonated triazole ring as calculated by natural population analysis with a large basis set ( $CH_{\text{triaz}}$ ) because this parameter proved to be robust and yields a good correlation ( $r = 0.96$ ) with the Hammett  $\sigma$  constants for 15 compounds for which a  $\sigma$  is available<sup>90</sup> (1, 4–17).

Of the 39 active triazoles described in this work, six could not satisfactorily be docked into the IDO1 active site because of

bulky substituents in *para* or *meta* positions (compounds 5, 6, 7, 13, 36, and 37, see filtering conditions in the Experimental Section) and were therefore removed from the test set. For the remaining set of 33 compounds, we obtained the best QSAR model when using two simple parameters in the regression analysis: the sum of the ligand–protein electrostatic interaction energy and the electrostatic desolvation energy on the one hand ( $V_{\text{elec}}$ ), and the quantum chemical charge on the triazole ( $CH_{\text{triaz}}$ ) on the other hand. With these two parameters a correlation coefficient of 0.87 and a standard deviation of 0.73 kcal/mol is obtained (Figure 4C).

$$Act = -38.79 + 0.60 \times V_{\text{elec}} - 34.48 \times CH_{\text{triaz}} \quad (2)$$

where  $Act$  and  $V_{\text{elec}}$  are given in kcal/mol and  $CH_{\text{triaz}}$  is given in elementary charge units. Compound 35 has a prominent location on the correlation plot (Figure 4C). However, its omission from the test set only marginally changes the correlation ( $r = 0.85$ ,  $stdv = 0.73$  kcal/mol). Addition of terms for the van de Waals interactions and hydrophobic desolvation does not improve the correlation, probably because these terms show little variation between the described compounds, which all tightly occupy only the A-pocket of the IDO1 active site.



**Figure 5.** Ligand efficiency [kcal/mol/atom] of known IDO1 ligands (blue) and the compounds described in this work (red). Ligands that probably interact with the cystein residues of IDO1<sup>44,49</sup> were not included. Indole-4,7-dione<sup>41</sup> probably acts through a redox mechanism.

**Table 5. Cellular Assays for IDO1 and TDO Inhibition<sup>a</sup>**

	enzym IC <sub>50</sub> [μM]		cell IC <sub>50</sub> [μM] <sup>b</sup>			LD <sub>50</sub> [μM]
	hIDO1	mIDO1	hIDO1	mTDO	hTDO	
1	83	0.18 (0.05)	8.9 (0.8)	>100	>100	>100
4	190	2.1 (1)	>100	>100	>100	>100
8	1.2	0.020 (0.003)	0.62 (0.01)	>100	>100	>100
9	2.0	0.023 (0.009)	0.94 (0.07)	>100	>100	>100
10	2.8	0.029 (0.006)	2.9 (0.6)	>100	>100	>100
11	6.0	0.07 (0.03)	9 (4)	>100	>100	>100
12	13	0.03 (0.02)	1.1 (0.1)	>100	>100	>100
13	15	0.11 (0.02)	24 (0.1)	>100	>100	>100
14	22	0.12 (0.04)	7 (3)	>100	>100	>100
15	47	1.1 (0.4)	>100	>100	>100	>100
16	310	1.3 (0.6)	>100	>100	>100	>100
17	1500	4 (2)	>100	>100	>100	>100
18	2.8	0.06 (0.02)	3.5 (0.5)	>100	>100	>100
19	3.3	0.05 (0.03)	2.9 (0.4)	>100	>100	>100
20	7.4	0.12 (0.01)	7 (1)	>100	>100	>100
21	15	0.34 (0.05)	56 (2)	>100	>100	>100
22	6.4	0.034 (0.001)	2.6 (0.1)	>100	>100	>100
23	15	0.022 (0.001)	1.7 (0.1)	>100	>100	>100
24	32	1.5 (0.3)	>100	>100	>100	>100
25	39	1.7 (0.1)	>100	>100	>100	>100
26	60	1.7 (0.4)	>100	>100	>100	>100
27	80	0.63 (0.09)	70 (20)	>100	>100	>100
28	230	13 (2)	>100	>100	>100	>100
29	650	20 (1)	>100	>100	>100	>100
32	NI	20 (1)	>100	>100	>100	>100
35	0.33	0.002 (0.002)	0.08 (0.02)	>100	>100	>100
36	4.3	0.12 (0.04)	14 (4)	>100	>100	>100
37	6.4	0.15 (0.04)	34 (2)	>100	>100	>100
38	23	1.7 (0.1)	>100	>100	>100	>100
Incyte 51 <sup>51</sup>	ND	0.10 (0.07)	0.06 (0.03)	60 (30)	70 (20)	>100
LM10 <sup>18</sup>	ND	>100	>100	17	28	>100

<sup>a</sup>IC<sub>50</sub> values of compounds tested in cells transfected with mouse IDO1 (mIDO1), human IDO1 (hIDO1), mouse TDO (mTDO), or human TDO (hTDO). Standard deviations are given in parentheses. Cytotoxicity of the compounds was tested on Hep G2 cells (LD<sub>50</sub>). For comparison, also the IC<sub>50</sub> values of the enzymatic assay on hIDO1 are given again. ND: not determined. NI: no inhibition. <sup>b</sup>IC<sub>50</sub> values are the mean of at least two independent assays.

It is important to notice that the QSAR model does not rely on either the heme-binding strength or the deprotonation hypothesis, but it is valid for both cases.

According to this model, compound 35 is highly active on IDO1 because it displays very good electrostatic interactions with the protein while carrying a low charge on the triazole

ring. Interestingly, in the docked pose (Figure 2N), there is no intramolecular hydrogen bond present, but the hydroxyl group forms a hydrogen bond with Ser167 instead. As MMG-0358 (compound 35) is very small, it shows an excellent ligand efficiency<sup>96</sup> of  $-0.72$  kcal/mol/atom, ranking among the most efficient IDO1 inhibitors known to date (Figure 5).

#### Comparison to Imidazole and Pyrazole Analogues.

Although compound 1 is a close analogue of PIM and docks in a similar manner to IDO1, the triazoles and imidazoles differ substantially in their structure–activity relationship for IDO1 inhibition. For example, the disubstituted imidazole compound 1-benzyl-5-phenylimidazole shows a slightly better  $IC_{50}$  value than PIM (32 vs 48  $\mu$ M),<sup>46</sup> while the direct analogue 1-benzyl-5-phenyl-1,2,3-triazole (56) is inactive. Replacement of the phenyl ring by a *p*-pyridyl ring in the triazole (2) leaves its activity unaffected, while the same replacement in the imidazole strongly reduces its activity (67). Despite these dissimilarities, there are also similarities, as the general drop in activity when introducing substituents in *para* position of the phenyl ring, and the much higher activity of compounds with *ortho*-hydroxyl as compared to *meta*-hydroxyl substituted phenyl rings.<sup>46</sup> While the similarities are probably due to the similar binding modes and similar protein interactions in the IDO1 active site, the differences can be explained by distinctive electronic structures and heme interactions. PIM is a much stronger base and a much weaker acid than compound 1 (Table 4), which correlates with the higher charge density on the heme-binding nitrogen of the imidazole (charge  $-0.46$ ) as compared to 1,2,3-triazole ( $-0.24$  neutral,  $-0.35$  deprotonated). It is therefore active on IDO1 without deprotonation, so that the N3 position is available for additional substitutions, and so that electron-withdrawing substituents on the phenyl ring do not show the same effect as in case of the triazoles.

A close analogue of compound 35 is the previously published 4-fluoro-2-(pyrazol-3-yl)phenol, featuring a pyrazole with a 2-OH,5-F substituted phenyl ring and an  $IC_{50}$  value of 26  $\mu$ M.<sup>46</sup> The about 100-fold higher activity of compound 35 on IDO1 could be explained by the better protein interactions of chloride vs fluoride and by the stronger heme bond of the triazole ( $-14.8$  kcal/mol) vs the pyrazole ( $-8.4$  kcal/mol, see Supporting Information).

**Cellular Assays.** We tested compounds with a low  $IC_{50}$  in the enzymatic assay for their ability to inhibit tryptophan degradation and kynurenine production in cells expressing either murine (mIDO1) or human IDO1 (hIDO1). Such cellular assay is informative for drug development, as it evaluates not only the IDO1 inhibitory effect of the compounds but also their capacity to permeate the cell, their potential cytotoxicity, inhibition of tryptophan and kynurenine transport, and interactions with other proteins as well as the effects of their metabolites. To control specificity, we also tested the inhibitory activity of the compounds on cells expressing murine (mTDO) or human TDO (hTDO). The same murine cell type, stably transfected with murine or human IDO1 or TDO, was used for all assays. Additionally, cell viability was evaluated using Hep G2 cells.

Most compounds active in the enzymatic assay were also active in the cellular assay, usually with lower  $IC_{50}$  values (Table 5 and Figure 4D), in line with previous observations.<sup>51,54</sup> In the present case this might be due to the higher pH employed in the cellular assays (7.4) as compared to the enzymatic assays (6.5), favoring deprotonation of the triazole ligands. The  $IC_{50}$  values for the triazole compounds are in the micromolar to

nanomolar range, with a good selectivity as no inhibition was observed in TDO-expressing cells. Strikingly, we consistently observed substantially higher inhibitory activities in the cellular assay performed with murine IDO1 as compared to human IDO1, with  $IC_{50}$  values on average 77-fold lower. This was not related to the cell type because we used the same murine cell line transfected with mIDO1 or hIDO1 for these assays. We also used human cells HEK293 transfected with hIDO1 and observed similar  $IC_{50}$  values as with the murine cells transfected with hIDO1 (data not shown). These differences therefore likely reflect genuine variation in the inhibition of murine versus human IDO1 by this family of compounds. Murine IDO1 shares 62% of sequence identity with human IDO1, and the active site residues mentioned in the Introduction are 100% conserved. However, the orthologues show some distinct biochemical properties, as, for example, mIDO1 displays a 3-fold lower  $K_m$  for L-Trp than hIDO1.<sup>97</sup> Despite these differences, an excellent correlation between the cellular assays on mIDO1 and on hIDO1 is observed ( $r = 0.95$ ). Additionally, the observed good correlation between enzymatic and cellular assay results (Figure 4D,  $r = 0.71$  for enzym. hIDO1/cell. hIDO1, and  $r = 0.79$  for enzym. hIDO1/cell. mIDO1) enables application of the developed QSAR model also for optimization of cellular activities.

The most promising IDO1 inhibitor reported to date is Incyte compound 51,<sup>51</sup> with  $IC_{50}$  values of 67 nM in an enzymatic assay and 19 nM in a cellular assay on HeLa cells. In our cellular assays, compound 35 displays a similar inhibitory effect on hIDO1 as 51 (80 and 60 nM respectively, Table 5) and therefore ranks among the most potent IDO1 inhibitors described so far.

## SUMMARY

In this work, we have used an *in silico* driven strategy for the rational optimization of IDO1 inhibitors based on the 4-aryl-1,2,3-triazole scaffold discovered in our earlier work.<sup>53</sup>

New ligands were designed computationally, docked into the IDO1 active site, selected in case of favorable interactions, synthesized, and evaluated for IDO1 inhibition potency in an enzymatic assay. Successful candidates were subsequently tested in cellular assays on mIDO1, hIDO1, mTDO, and hTDO. Bioisosteres of the 4-phenyl-1,2,3-triazole scaffold were also investigated. Using the results of the enzymatic assay, we developed a QSAR model based on the docking results and on quantum chemical calculations. Following this strategy, we obtained 39 triazole-based IDO1 inhibitors, the most potent having an  $IC_{50}$  value in the nanomolar range both in the enzymatic and in the cellular assays while being inactive on TDO and showing no detectable toxicity on the cellular level.

Some modifications of the 4-aryl-1,2,3-triazole scaffold have very recently been described independently by another group.<sup>54</sup> Among the 20 compounds described in their work, two were described by us before (1 and 3) and seven were also synthesized and tested in the present work (4, 5, 6, 22, 24, 32, and 65), while the remaining 11 compounds are either only weakly active or inactive. The enzymatic  $IC_{50}$  values measured in our lab generally differ by a factor 2–3 from the values of Huang et al., which is probably due to different experimental conditions. The only outlier is compound 22, for which the  $IC_{50}$  values differ significantly (148<sup>54</sup> vs 7  $\mu$ M here). The inhibition mode of compounds 1, 22, and 24 was determined to be uncompetitive.<sup>54</sup> However, the UV spectra of IDO1 in

presence of compound **35** measured here (Figure 3) support the notion that the triazoles bind directly to the heme iron.

As the compounds described in this work are very small, they might suffer from a low selectivity profile. However, their low cellular toxicity and inactivity on TDO, which shares a common active site architecture with IDO1, support their further development.

In summary, we have used our in-house docking tools to successfully design new IDO1 inhibitors with a good efficacy in enzymatic and in cellular assays. Our most potent compound (MMG-0358, **35**) shows IC<sub>50</sub> values of 2 nM in a cellular assay on mIDO1, 80 nM in a cellular assay on hIDO1, 330 nM in an enzymatic assay on hIDO1 at pH 6.5, and 71 nM in an enzymatic assay on hIDO1 at pH 7.4. This compound, which additionally has an excellent ligand efficiency<sup>96</sup> of  $-0.72$  kcal/mol/atom, will be evaluated in vivo in the future. The QSAR model derived from the collection of our evaluated ligands will be helpful in the future to design even more potent and specific IDO1 inhibitors.

## EXPERIMENTAL SECTION

**Docking.** A consensus docking procedure based on our in-house docking algorithms EADock,<sup>55,56</sup> EADock DSS,<sup>57</sup> and AttractingCavities<sup>70</sup> was used. In the latter, in brief, an extended conformation of the ligand is minimized in the cavities of the protein, starting from different positions and orientations, in an approach similar to that of MCSS.<sup>98</sup> Minimized poses are finally clustered and ranked according to the scoring function of EADock. A detailed description of this algorithm will be the subject of a future communication.

All three algorithms rely on the physical scoring function of the CHARMM22 force field,<sup>93,94</sup> while solvation effects are taken into account by the FACTS model,<sup>95</sup> which has been shown to allow for accurate docking results.<sup>59</sup> Ligand force-field parameters were derived with the SwissParam tool.<sup>60</sup> For all compounds with an acidic pK<sub>a</sub> value of 9.5 or below, the deprotonated species was considered. A Morse-like metal binding potential (MMBP) was used to describe the interactions between the heme iron of IDO1 and ligand atoms that display a free electron pair for iron binding.<sup>61</sup> The protein was kept fixed during the docking. We use the PIM-bound X-ray structure (2D0T, chain A) as a target because it has a higher resolution and provides a more suitable induced fit for the triazole ligands than the cyanide-bound structure (2D0U).<sup>25</sup> The two molecules of *N*-cyclohexyltaurine bound at the entrance of the binding site were removed during setup.

For AttractingCavities, the standard parameters with a cubic search space of (20 Å)<sup>3</sup> around the IDO1 active site were used. For EADock DSS, docking results were compared to EADock 2.0 results, and in order to well reproduce the benchmarks, the following custom settings were used: 30000 generated binding modes (BM), 12000 BM evaluated with FullFitness, 100 steepest descent minimization steps, 1000 adopted basis Newton–Raphson minimization steps, 1.5 Å clustering radius, and a cubic search space of (20 Å)<sup>3</sup> around the IDO1 active site. Subsequently, the 250 best BM produced by EADock DSS were fed as input to EADock 2.0, using the same clustering radius and terminating the run when the first three clusters did not change over the course of 100 generations of the evolutionary algorithm.

For analysis, the results of AttractingCavities and EADock 2.0 were merged by comparing the best BM of each cluster and considering them distinct if their mass-weighted rmsd was larger than 0.8 Å. The resulting 10 best distinct BM were filtered to detect energetically favorable poses with a direct bond to the heme iron and a good filling of the A-pocket, criteria that were deemed necessary for IDO1 inhibition by the investigated scaffold. The following filters were applied: (i) a FullFitness that is maximally 5 kcal/mol higher than the one of the globally best BM, (ii) an iron-heteroatom (N, O, S) bond of 3 Å or shorter, (iii) a minimal distance between the ligand and the sulfur atom of Cys129 of less than 5.2 Å, and (iv) a volume filling of

the A-pocket of at least 75%. Finally, for each compound the BM having the lowest FullFitness and meeting all conditions was chosen for analysis.

**Density Functional Theory Calculations.** Quantum chemical geometry optimizations and charge calculations were carried out in the density functional theory (DFT) framework with the PBE0 hybrid functional<sup>99</sup> using the Gaussian 09 code.<sup>100</sup> Geometry optimizations were carried out with standard settings and the TZVP basis set,<sup>101</sup> while atomic point charges derived from a natural population analysis (NPA)<sup>102</sup> were calculated with the aug-cc-pVTZ basis set<sup>103–105</sup> in order to obtain converged charges.<sup>106</sup> Solvation effects were taken into account by the polarizable continuum model<sup>92</sup> as implemented in Gaussian 09.

For compound **1**, the 2-H tautomer was the most stable both in vacuo and in the PCM. For charge calculations for the QSAR, compounds with an acidic pK<sub>a</sub> value of 9.5 or below were considered in their deprotonated form.

The histidine-bound heme complex of IDO1 was modeled by an iron–porphyrin–imidazole system. Binding energies were calculated by subtracting the energy of the iron–porphyrin–imidazole system and the energy of the isolated ligand from the energy of the 6-fold coordinated system. For the ferric iron–porphyrin–imidazole system, the ground state with the hybrid DFT functional PBE0 is a quartet, while for the ferrous system it is a quintuplet. For the 6-fold coordinated systems, a low-spin complex was always assumed, as it has been found experimentally.<sup>32</sup>

**Quantitative Structure–Activity Relationship.** The binding free energy  $\Delta G$  of an inhibitor is related to its K<sub>i</sub> value by the equation  $\Delta G = -RT \ln K_i$ . As the K<sub>i</sub> of an inhibitor is linearly related to its IC<sub>50</sub> value and the prefactor only depends on enzyme concentration, substrate concentration, and K<sub>m</sub> of the substrate,<sup>107,108</sup> we can calculate the activity of an inhibitor as  $Act = -RT \ln IC_{50}$ . Differences in the calculated activities of different inhibitors will then be equal to  $\Delta\Delta G$ .

For the QSAR model, we carried out a linear regression with two variables, using the activities as target values. The first variable is the sum of the NPA charges of all atoms belonging to the deprotonated triazole ring. The second variable,  $V_{elec}$  is

$$V_{elec} = \Delta G_{solv,elec} + E_{inter,elec} - E_{corr,elec} \quad (3)$$

with the electrostatic solvation term

$$\Delta G_{solv,elec} = \Delta G_{solv,elec}^{complex} - \Delta G_{solv,elec}^{ligand} - \Delta G_{solv,elec}^{protein} \quad (4)$$

as calculated by the FACTS solvation model.<sup>95</sup>  $E_{inter,elec}$  is the electrostatic interaction energy between the ligand and the protein calculated with the Coulomb equation and a dielectric constant of 2 as appropriate for the use of FACTS.  $E_{corr,elec}$  is a correction term necessary to counterbalance the use of the MMBP and equals the electrostatic interaction energy between the ligand on the one hand and the iron and nitrogen atoms of the heme on the other hand.

**Chemistry. General Remarks.** Materials and reagents were obtained from commercial suppliers and used without further purification. For extraction and chromatography, all solvents were distilled prior to use. Thin layer chromatography for reaction monitoring was performed on silica gel plates (Merck 60 F254) with detection by UV light (254 nm) and charring with KMnO<sub>4</sub> or Pancaldi reagent. Flash chromatography was conducted using silica gel 60 Å, 230–400 mesh (Merck 9385). Melting points were measured with a Mettler FP52 apparatus and are uncorrected. IR spectra were recorded on a Perkin-Elmer Paragon 1000 FT-IR spectrometer. Mass spectra were recorded on a Nermag R 10–10C instrument in chemical ionization mode. Electrospray mass analyses were recorded on a Finnigan MAT SSQ 710C spectrometer in positive ionization mode. <sup>1</sup>H and <sup>13</sup>C NMR spectra were recorded on a Bruker-DPX-400 or Bruker-ARX-400 spectrometer at 400 and 100.6 MHz, respectively. Data for <sup>1</sup>H NMR spectra are reported as follows: chemical shift, multiplicity, coupling constant, and integration. Data for <sup>13</sup>C NMR spectra are reported in terms of chemical shifts. Chemical shifts are given in parts per million, relative to an internal standard such as

residual solvent signals. Coupling constants are given in hertz. High-resolution mass spectra were recorded via ESI-TOF-HRMS or MALDI-TOF-HRMS. The purity of all novel compounds was confirmed to exceed 95% by NMR and high-resolution mass spectra. Elemental analysis for C, H, and N was performed by Quantitative Technologies Inc.

**General Procedures. Representative Procedure for the Preparation of Phenylalkynes.**<sup>72</sup> To a stirred solution of iodo derivative (Scheme 1, A, 1 mmol, 1 equiv) and Et<sub>3</sub>N (4 mmol, 4 equiv) in dioxane (4 mL) were added trimethylsilyl acetylene (1.3 mmol, 1.3 equiv), PdCl<sub>2</sub>(PPh<sub>3</sub>)<sub>2</sub> (0.01 mmol, 0.01 equiv), and CuI (0.02 mmol, 0.02 equiv). The reaction mixture was stirred at 45 °C for 5 h under nitrogen. Diethyl ether (5 mL) and 0.1 N HCl (3 mL) were added, and the organic layer was separated, neutralized with a saturated NaHCO<sub>3</sub> (3 mL, twice) solution, washed with brine (3 mL), dried over Na<sub>2</sub>SO<sub>4</sub>, and evaporated. The residue (B) was added to KF (3.6 mmol, 3.6 equiv) dissolved in MeOH (5 mL), and the reaction mixture was stirred for 3 h at room temperature. The reaction mixture was concentrated, and CH<sub>2</sub>Cl<sub>2</sub> (5 mL) and water (3 mL) were added. The organic layer was collected, dried (MgSO<sub>4</sub>), and filtered through a short silica plug to afford desired (ethynyl) derivative (C) compounds; overall yields up to 85%.

**2-Ethynylphenol.**<sup>72</sup> Synthesized from 2-iodophenol according to the representative procedure<sup>72</sup> to afford the title compound as a yellowish oil in 85% yield. <sup>1</sup>H NMR (400 MHz, CDCl<sub>3</sub>): δ 7.40 (dd, 1H, J = 7.5 Hz, 1.7 Hz), 7.33–7.30 (m, 1H), 6.98 (d, 1H, J = 8.5 Hz), 6.90 (td, 1H, J = 7.5 Hz, 1.0 Hz), 5.81 (s, 1H), 3.50 (s, 1H).

**1-Ethyl-2-ethynylbenzene.**<sup>109</sup> Synthesized from 1-ethyl-2-iodobenzene according to the representative procedure<sup>72</sup> to afford the title compound as a yellow oil in 80% yield. <sup>1</sup>H NMR (400 MHz, CDCl<sub>3</sub>): δ 7.48 (d, 1H, J = 7.5 Hz, 1.7 Hz), 7.29 (td, 1H, J = 7.4 Hz, 1.5 Hz), 7.23 (d, 1H, J = 7.1 Hz), 7.15 (td, 1H, J = 7.5 Hz, 1.2 Hz), 3.25 (s, 1H), 2.84 (q, 2H, J = 7.5 Hz), 1.26 (t, 3H, J = 7.5 Hz).

**3-Ethynylbenzonitrile.**<sup>110</sup> Synthesized from 2-iodobenzonitrile according to the representative procedure<sup>72</sup> to afford the title compound as a yellow oil in 80% yield. <sup>1</sup>H NMR (400 MHz, CDCl<sub>3</sub>): δ 7.79 (s, 1H), 7.73 (dt, 1H, J = 7.9 Hz, 1.3 Hz), 7.66 (dt, 1H, J = 7.9 Hz, 1.3 Hz), 7.48 (t, 1H, J = 7.9 Hz), 3.22 (s, 1H).

**1-Ethyl-3-ethynylbenzene.**<sup>111</sup> Synthesized from 1-ethyl-3-iodobenzene according to the representative procedure<sup>72</sup> to afford the title compound as yellow oil in 75% yield. <sup>1</sup>H NMR (400 MHz, CDCl<sub>3</sub>): δ 7.36–7.30 (m, 2H), 7.25–7.14 (m, 2H), 3.06 (s, 1H), 2.64 (q, 2H, J = 7.5 Hz), 1.24 (t, 3H, J = 7.6 Hz).

**4-Ethynyl-2-fluoropyridine.**<sup>112</sup> Synthesized from 2-fluoro-4-iodopyridine according to the representative procedure<sup>72</sup> to afford the title compound as colorless oil in 65% yield. <sup>1</sup>H NMR (400 MHz, CDCl<sub>3</sub>): δ 8.21 (d, 1H, J = 5.0 Hz), 7.24 (d, 1H, J = 5.0 Hz), 7.01 (s, 1H), 3.38 (s, 1H).

**2-Chloro-4-ethynylpyridine.**<sup>113</sup> Synthesized from 2-chloro-4-iodopyridine according to the representative procedure<sup>72</sup> to afford the title compound as a yellow solid in 60% yield. <sup>1</sup>H NMR (400 MHz, CDCl<sub>3</sub>): δ 8.38 (d, 1H, J = 5.0 Hz), 7.41 (s, 1H), 7.28 (dd, 1H, J = 5.0 Hz, 1.2 Hz), 3.37 (s, 1H).

**1,2-Dichloro-3-ethynylbenzene.**<sup>114</sup> Synthesized from 1,2-dichloro-3-iodobenzene according to the representative procedure<sup>72</sup> to afford the title compound as brown semisolid in 65% yield. <sup>1</sup>H NMR (400 MHz, CDCl<sub>3</sub>): δ 7.46 (d, 2H, J = 8.0 Hz), 7.17 (t, 1H, J = 8.0 Hz), 3.38 (s, 1H).

**1,4-Dichloro-2-ethynylbenzene.**<sup>115</sup> Synthesized from 1,4-dichloro-2-iodobenzene according to the representative procedure<sup>72</sup> to afford the title compound as an off-white solid in 73% yield. <sup>1</sup>H NMR (400 MHz, CDCl<sub>3</sub>): δ 7.52 (d, 1H, J = 2.52 Hz), 7.34 (d, 1H, J = 8.5 Hz), 7.26 (dd, 1H, J = 8.5 Hz, 2.5 Hz), 3.42 (s, 1H).

**2-Ethynyl-N-methylaniline.**<sup>116</sup> Synthesized from 2-iodo-N-methylaniline according to the representative procedure<sup>72</sup> to afford the title compound as a brown oil in 72% yield. <sup>1</sup>H NMR (400 MHz, CDCl<sub>3</sub>): δ 7.34 (dd, 1H, J = 7.6 Hz, 1.5 Hz), 7.28–7.23 (m, 1H), 6.65–6.58 (m, 2H), 4.68 (bs, 1H), 3.41 (s, 1H), 2.91 (s, 3H).

**2-Ethynylbenzaldehyde.**<sup>117</sup> Synthesized from 2-iodobenzaldehyde according to the representative procedure<sup>72</sup> to afford the title

compound as an off-white solid in 85% yield. <sup>1</sup>H NMR (400 MHz, CDCl<sub>3</sub>): δ 10.55 (s, 1H), 7.94 (d, 1H, J = 7.6 Hz), 7.63 (dd, 1H, J = 7.2, Hz, 1.1 Hz), 7.58 (td, 1H, J = 7.5 Hz, 1.5 Hz), 7.49 (t, 1H, J = 7.6 Hz), 3.47 (s, 1H).

**3-Ethynyl-4-methylaniline.**<sup>118</sup> Synthesized from 3-iodo-4-methylaniline according to the representative procedure<sup>72</sup> to afford the title compound as a brown oil in 70% yield. <sup>1</sup>H NMR (400 MHz, CDCl<sub>3</sub>): δ 7.01 (d, 1H, J = 8.1 Hz), 6.85 (d, 1H, J = 2.5 Hz), 6.64 (dd, 1H, J = 5.5 Hz, 2.5 Hz), 3.67 (br s, 1H), 3.24 (s, 1H), 2.36 (s, 3H).

**4-Chloro-2-ethynylphenol.** Synthesized from 4-chloro-2-iodophenol according to the representative procedure<sup>72</sup> to afford the title compound as a colorless oil in 70% yield. <sup>1</sup>H NMR (400 MHz, CDCl<sub>3</sub>): δ 7.35 (d, 1H, J = 2.5 Hz), 7.24 (dd, 1H, J = 8.7 Hz, 2.5 Hz), 6.90 (d, 1H, J = 8.8 Hz), 5.76 (s, 1H), 3.52 (s, 1H).

**4-Chloro-2-ethynyl-1-methylbenzene.**<sup>119</sup> Synthesized from 4-chloro-2-iodo-1-methylbenzene according to the representative procedure<sup>72</sup> to afford the title compound as a yellow oil in 60% yield. <sup>1</sup>H NMR (400 MHz, CDCl<sub>3</sub>): δ 7.46 (d, 1H, J = 2.2 Hz), 7.24 (dd, 1H, J = 6.0 Hz, 2.3 Hz), 7.15 (d, 1H, J = 8.1 Hz), 3.33 (s, 1H), 2.44 (s, 3H).

**General Procedure for N-Unsubstituted 1,2,3-Triazoles.**<sup>71</sup> To a stirred solution of commercially available or synthetically prepared ethynyl substrate (1 mmol, 1 equiv) and CuI (0.05 mmol, 0.05 equiv) in DMF/MeOH solution (2 mL, 9:1) under an argon atmosphere, trimethylsilyl azide was added (1.5 mmol, 1.5 equiv). The resulting solution was stirred at 100 °C for 10–12 h. After consumption of the ethynyl substrate, the mixture was cooled to room temperature and the precipitate was filtered and concentrated under reduced pressure. The crude residue was purified with silica gel column chromatography to obtain the desired product.

**General Procedure for the Preparation of Triazoles 48, 49, 50, 51, 52, and 53 by N-Alkylation of 4-Phenyl-1H-1,2,3-triazole.**<sup>82–84</sup> To a solution of 4-phenyl-1H-1,2,3-triazole (1 mmol, 1 equiv) in DMF (3 mL), K<sub>2</sub>CO<sub>3</sub> (0.25 mmol, 0.25 equiv) was added. The mixture was stirred for 5 min at room temperature. Dimethyl or diethyl carbonate (2.2 mmol, 2.2 equiv) was added, and the mixture was stirred at reflux (around 145 °C) for 5 h. The resulting solution was filtered, and the remaining solid material was washed with Et<sub>2</sub>O (5 mL). Evaporation of the solvent afforded an oily residue. From the crude oil the different regioisomers were separated by column chromatography on silica gel to give compounds 48, 49, 50, 51, 52, and 53 in 7, 60, 20, 6, 19, and 55% yield respectively.

**General Procedure for the Preparation of Triazoles 59 and 60 by N-Methylation of 4-(3-Chlorophenyl)-1H-1,2,3-triazole.**<sup>82</sup> To a solution of 8 (1 mmol, 1 equiv) in DMF (4 mL), K<sub>2</sub>CO<sub>3</sub> (1 mmol, 1 equiv) was added. The mixture was stirred for 5 min at room temperature. Iodomethane (1 mmol, 1 equiv) was added, and the mixture was stirred at room temperature for 24 h. The resulting solution was filtered, and the remaining solid material was washed with Et<sub>2</sub>O (4 mL). Evaporation of the solvent afforded an oily residue. From the crude oil, the different regioisomers were separated by column chromatography on silica gel to give compounds 59 and 60 in 7 and 60% yield, respectively.

**4-Phenyl-1H-1,2,3-triazole (1).**<sup>71</sup> Synthesized from ethynylbenzene<sup>71</sup> and TMSN<sub>3</sub> according to the general procedure to afford 1 as a white solid in 65% yield. <sup>1</sup>H NMR (400 MHz, CDCl<sub>3</sub>): δ 12.34 (br s, 1H), 8.00 (s, 1H), 7.84 (d, 2H, J = 7.6 Hz), 7.47 (t, 2H, J = 7.6 Hz), 7.43–7.37 (m, 1H).

**4-(1H-1,2,3-Triazol-4-yl)pyridine (2).**<sup>62</sup> Synthesized from 4-ethynylpyridine<sup>71</sup> and TMSN<sub>3</sub> according to the general procedure to afford 2 as a white solid in 40% yield. <sup>1</sup>H NMR (400 MHz, CD<sub>3</sub>OD): δ 8.60 (d, 2H, J = 6.0 Hz), 8.41 (br s, 1H), 7.91 (d, 2H, J = 6.0 Hz).

**3-(1H-1,2,3-Triazol-4-yl)pyridine (3).**<sup>62</sup> Synthesized from 3-ethynylpyridine<sup>71</sup> and TMSN<sub>3</sub> according to the general procedure to afford 3 as a white solid in 60% yield. <sup>1</sup>H NMR (400 MHz, CDCl<sub>3</sub>-CD<sub>3</sub>OD): δ 8.96 (s, 1H), 8.51 (d, 1H, J = 4.8 Hz), 8.14 (d, 1H, J = 7.8 Hz), 7.99 (s, 1H), 7.42–7.38 (m, 1H).

**4-(4-Fluorophenyl)-1H-1,2,3-triazole (4).**<sup>120</sup> Synthesized from 1-ethynyl-4-fluorobenzene<sup>71</sup> and TMSN<sub>3</sub> according to the general procedure to afford 4 as a white solid in 62% yield. <sup>1</sup>H NMR (400

MHz, CDCl<sub>3</sub>):  $\delta$  11.65 (s, 1H), 7.95 (s, 1H), 7.85–7.80 (m, 2H), 7.21–7.14 (m, 2H).

**4-(4-Chlorophenyl)-1H-1,2,3-triazole (5).**<sup>62</sup> Synthesized from 1-chloro-4-ethynylbenzene<sup>71</sup> and TMSN<sub>3</sub> according to the general procedure to afford **5** as a white solid in 65% yield. <sup>1</sup>H NMR (400 MHz, CDCl<sub>3</sub>):  $\delta$  11.66 (s, 1H), 7.98 (s, 1H), 7.79 (d, 2H,  $J$  = 8.4 Hz), 7.46 (d, 2H,  $J$  = 8.4 Hz).

**4-(*p*-Tolyl)-1H-1,2,3-triazole (6).**<sup>62</sup> Synthesized from 1-ethynyl-4-methylbenzene<sup>71</sup> and TMSN<sub>3</sub> according to the general procedure to afford **6** as a white solid in 72% yield. <sup>1</sup>H NMR (400 MHz, CD<sub>3</sub>OD):  $\delta$  8.07 (s, 1H), 7.69 (d, 2H,  $J$  = 7.9 Hz), 7.24 (d, 2H,  $J$  = 7.9 Hz), 2.35 (s, 3H).

**4-(4-(Trifluoromethyl)phenyl)-1H-1,2,3-triazole (7).**<sup>121</sup> Synthesized from 1-ethynyl-4-(trifluoromethyl)benzene<sup>71</sup> and TMSN<sub>3</sub> according to the general procedure to afford **7** as a white solid in 55% yield. <sup>1</sup>H NMR (400 MHz, CDCl<sub>3</sub>):  $\delta$  11.77 (s, 1H), 8.06 (s, 1H), 7.98 (d, 2H,  $J$  = 8.2 Hz), 7.74 (d, 2H,  $J$  = 8.2 Hz).

**4-(3-Chlorophenyl)-1H-1,2,3-triazole (8).**<sup>121</sup> Synthesized from 1-chloro-3-ethynylbenzene<sup>71</sup> and TMSN<sub>3</sub> according to the general procedure to afford **8** as a white solid in 70% yield. <sup>1</sup>H NMR (400 MHz, CDCl<sub>3</sub>):  $\delta$  11.79 (s, 1H), 8.0 (s, 1H), 7.86 (s, 1H), 7.74 (d, 2H,  $J$  = 7.5 Hz), 7.45–7.36 (m, 2H).

**4-(3-Bromophenyl)-1H-1,2,3-triazole (9).**<sup>62</sup> Synthesized from 1-bromo-3-ethynylbenzene<sup>71</sup> and TMSN<sub>3</sub> according to the general procedure to afford **9** as a white solid in 68% yield. <sup>1</sup>H NMR (400 MHz, CDCl<sub>3</sub>):  $\delta$  11.87 (s, 1H), 8.02 (s, 1H), 8.0 (s, 1H), 7.78 (d, 1H,  $J$  = 7.8 Hz), 7.53 (d, 1H,  $J$  = 8.1 Hz), 7.35 (t, 1H,  $J$  = 8.0 Hz).

**3-(1H-1,2,3-Triazol-4-yl)benzotrile (10).**<sup>122</sup> Synthesized from 3-ethynylbenzotrile<sup>71</sup> and TMSN<sub>3</sub> according to the general procedure to afford **10** as a off-white solid in 54% yield. <sup>1</sup>H NMR (400 MHz, CDCl<sub>3</sub>):  $\delta$  11.73 (s, 1H), 8.16 (s, 1H), 8.09 (d, 1H,  $J$  = 7.8 Hz), 8.04 (s, 1H), 7.71–7.65 (m, 1H), 7.60 (t, 1H,  $J$  = 7.8 Hz).

**4-(3-(Trifluoromethyl)phenyl)-1H-1,2,3-triazole (11).**<sup>123</sup> Synthesized from 1-ethynyl-3-(trifluoromethyl)benzene<sup>71</sup> and TMSN<sub>3</sub> according to the general procedure to afford **11** as a white solid in 55% yield. <sup>1</sup>H NMR (400 MHz, CDCl<sub>3</sub>):  $\delta$  11.85 (s, 1H), 8.12 (s, 1H), 8.06 (s, 1H), 8.04 (d, 1H,  $J$  = 7.8 Hz), 7.67 (d, 1H,  $J$  = 7.9 Hz), 7.61 (t, 1H,  $J$  = 7.8 Hz).

**4-(3-Ethylphenyl)-1H-1,2,3-triazole (12).** Synthesized from 1-ethyl-3-ethynylbenzene<sup>71</sup> and TMSN<sub>3</sub> according to the general procedure to afford **12** as a yellow oil in 71% yield. IR (film):  $\nu$  3136, 2964, 1613, 1476, 796 cm<sup>-1</sup>. <sup>1</sup>H NMR (400 MHz, CDCl<sub>3</sub>):  $\delta$  11.90 (s, 1H), 8.0 (s, 1H), 7.70 (br s, 1H), 7.65 (d, 1H,  $J$  = 7.5 Hz), 7.40 (t, 1H,  $J$  = 7.7 Hz), 7.26 (d, 1H,  $J$  = 7.7 Hz). <sup>13</sup>C NMR (100 MHz, CDCl<sub>3</sub>):  $\delta$  147.0, 145.2, 129.6, 129.1, 128.5, 125.8, 123.6, 29.0, 15.6. ESI-TOF-HRMS:  $m/z$  calcd for (M + H) C<sub>10</sub>H<sub>11</sub>N<sub>3</sub>, 174.1031; found, 174.1024.

**4-(3-Nitrophenyl)-1H-1,2,3-triazole (13).**<sup>124</sup> Synthesized from 1-ethynyl-3-nitrobenzene<sup>71</sup> and TMSN<sub>3</sub> according to the general procedure to afford **13** as a off-white solid in 58% yield. <sup>1</sup>H NMR (400 MHz, CDCl<sub>3</sub>):  $\delta$  8.60 (s, 1H), 8.23–8.11 (m, 2H), 8.02 (s, 1H), 7.62 (t, 1H,  $J$  = 8.0 Hz).

**4-(*m*-Tolyl)-1H-1,2,3-triazole (14).**<sup>62</sup> Synthesized from 1-ethynyl-3-methylbenzene<sup>71</sup> and TMSN<sub>3</sub> according to the general procedure to afford **14** as a white solid in 62% yield. <sup>1</sup>H NMR (400 MHz, CDCl<sub>3</sub>):  $\delta$  11.88 (s, 1H), 8.0 (s, 1H), 7.68 (s, 1H), 7.64 (d, 1H,  $J$  = 7.6 Hz), 7.37 (t, 1H,  $J$  = 7.7 Hz), 7.23 (d, 1H,  $J$  = 7.6 Hz), 2.45 (s, 3H).

**4-(3-Fluorophenyl)-1H-1,2,3-triazole (15).**<sup>125</sup> Synthesized from 1-ethynyl-3-fluorobenzene<sup>71</sup> and TMSN<sub>3</sub> according to the general procedure to afford **15** as a white solid in 51% yield. <sup>1</sup>H NMR (400 MHz, CD<sub>3</sub>OD):  $\delta$  8.21 (s, 1H), 7.67 (d, 1H,  $J$  = 7.8 Hz), 7.63–7.58 (m, 1H), 7.50–7.43 (m, 1H), 7.10 (td, 1H,  $J$  = 8.5 Hz, 2.5 Hz).

**3-(1H-1,2,3-Triazol-4-yl)phenol (16).**<sup>62</sup> Synthesized from 3-ethynylphenol<sup>71</sup> and TMSN<sub>3</sub> according to the general procedure to afford **16** as a light-yellow powder in 20% yield. <sup>1</sup>H NMR (400 MHz, CD<sub>3</sub>OD):  $\delta$  8.08 (s, 1H), 7.32–7.22 (m, 3H), 6.83–6.77 (m, 1H).

**3-(1H-1,2,3-Triazol-4-yl)aniline (17).**<sup>62</sup> Synthesized from 3-ethynylaniline<sup>71</sup> and TMSN<sub>3</sub> according to the general procedure to afford **17** as a light-yellow powder in 55% yield. <sup>1</sup>H NMR (400 MHz, CD<sub>3</sub>OD):  $\delta$  8.06 (s, 1H), 7.22–7.12 (m, 3H), 6.77–6.72 (m, 1H).

**2-Chloro-4-(1H-1,2,3-triazol-4-yl)pyridine (18).** Synthesized from 2-chloro-4-ethynylpyridine<sup>71</sup> and TMSN<sub>3</sub> according to the general procedure to afford **18** as a off-white solid in 60% yield, mp 211–213 °C. IR (film):  $\nu$  3121, 2171, 1604, 1454, 1070, 998, 838 cm<sup>-1</sup>. <sup>1</sup>H NMR (400 MHz, CD<sub>3</sub>OD):  $\delta$  8.45 (br s, 1H), 8.43 (d, 1H,  $J$  = 5.6 Hz), 7.96 (s, 1H), 7.86 (d, 1H,  $J$  = 5.38 Hz). <sup>13</sup>C NMR (100 MHz, CD<sub>3</sub>OD):  $\delta$  151.8, 149.9, 142.9, 142.0, 120.2, 119.0. ESI-TOF-HRMS:  $m/z$  calcd for (M + H) C<sub>7</sub>H<sub>5</sub>ClN<sub>4</sub>, 181.0281; found, 181.0275.

**2-Bromo-4-(1H-1,2,3-triazol-4-yl)pyridine (19).** Synthesized from 2-bromo-4-ethynylpyridine<sup>71</sup> and TMSN<sub>3</sub> according to the general procedure to afford **19** as a white solid in 61% yield, mp 206–209 °C. IR (film):  $\nu$  3126, 2138, 1601, 1530, 1068, 834 cm<sup>-1</sup>. <sup>1</sup>H NMR (400 MHz, CD<sub>3</sub>OD):  $\delta$  8.44 (s, 1H), 8.39 (d, 1H,  $J$  = 5.4 Hz), 8.11 (s, 1H), 7.88 (d, 1H,  $J$  = 5.3 Hz). <sup>13</sup>C NMR (100 MHz, DMSO):  $\delta$  151.6, 142.8, 142.6, 141.6, 124.0, 119.9. ESI-TOF-HRMS:  $m/z$  calcd for (M + H) C<sub>7</sub>H<sub>5</sub>BrN<sub>4</sub>, 224.9776; found, 224.9771.

**2-Fluoro-4-(1H-1,2,3-triazol-4-yl)pyridine (20).** Synthesized from 4-ethynyl-2-fluoropyridine<sup>71</sup> and TMSN<sub>3</sub> according to the general procedure to afford **20** as a off-white solid in 62% yield, mp 197–199 °C. IR (film):  $\nu$  3138, 2918, 2263, 1618, 1417, 1212, 1074, 830 cm<sup>-1</sup>. <sup>1</sup>H NMR (400 MHz, CDCl<sub>3</sub>-CD<sub>3</sub>OD):  $\delta$  8.23 (d, 1H,  $J$  = 5.3 Hz), 8.03 (s, 1H), 7.62–7.51 (m, 1H), 7.37 (s, 1H). <sup>13</sup>C NMR (100 MHz, CD<sub>3</sub>OD):  $\delta$  164.5 (d,  $J$  = 237.2 Hz), 147.9, 147.7, 144.3 (d,  $J$  = 8.8 Hz), 118.1 (d,  $J$  = 3.7 Hz), 105.4, 105.0. ESI-TOF-HRMS:  $m/z$  calcd for (M + H) C<sub>7</sub>H<sub>5</sub>FN<sub>4</sub>, 165.0576; found, 165.0583.

**4-(1H-1,2,3-Triazol-4-yl)-2-(trifluoromethyl)pyridine (21).** Synthesized from 4-ethynyl-2-(trifluoromethyl)pyridine<sup>71</sup> and TMSN<sub>3</sub> according to the general procedure to afford **21** as a white solid in 51% yield, mp 211–213 °C. IR (film):  $\nu$  3147, 3098, 2885, 2160, 1618, 1321, 1112, 707 cm<sup>-1</sup>. <sup>1</sup>H NMR (400 MHz, CD<sub>3</sub>OD):  $\delta$  8.76 (d, 1H,  $J$  = 5.0 Hz), 8.53 (br s, 1H), 8.29 (s, 1H), 8.11 (d, 1H,  $J$  = 5.2 Hz). <sup>13</sup>C NMR (100 MHz, CD<sub>3</sub>OD):  $\delta$  150.4, 148.4 (q,  $J$  = 34.16), 143.1, 140.6, 122.7, 121.6 (q,  $J$  = 274.7, 116.6 (q,  $J$  = 2.89). ESI-TOF-HRMS:  $m/z$  calcd for (M + H) C<sub>8</sub>H<sub>5</sub>F<sub>3</sub>N<sub>4</sub>, 215.0545; found, 215.0548.

**4-(2-Bromophenyl)-1H-1,2,3-triazole (22).**<sup>126</sup> Synthesized from 1-bromo-2-ethynylbenzene<sup>71</sup> and TMSN<sub>3</sub> according to the general procedure to afford **22** as a white solid in 55% yield. <sup>1</sup>H NMR (400 MHz, CD<sub>3</sub>OD):  $\delta$  8.26 (s, 1H), 7.76 (d, 1H,  $J$  = 7.4 Hz), 7.73 (d, 1H,  $J$  = 8.0 Hz), 7.46 (t, 1H,  $J$  = 7.5 Hz), 7.31 (t, 1H,  $J$  = 7.8 Hz).

**2-(1H-1,2,3-Triazol-4-yl)phenol (23).**<sup>127</sup> Synthesized from 2-ethynylphenol<sup>71</sup> and TMSN<sub>3</sub> according to the general procedure to afford **23** as a white solid in 32% yield. <sup>1</sup>H NMR (400 MHz, CDCl<sub>3</sub>):  $\delta$  11.77 (s, 1H), 8.10 (s, 1H), 7.63 (d, 1H,  $J$  = 7.6 Hz), 7.35–7.28 (m, 1H), 7.10 (d, 1H,  $J$  = 8.4 Hz), 7.0 (t, 1H,  $J$  = 7.8 Hz).

**4-(2-Chlorophenyl)-1H-1,2,3-triazole (24).**<sup>121</sup> Synthesized from 1-chloro-2-ethynylbenzene<sup>71</sup> and TMSN<sub>3</sub> according to the general procedure to afford **24** as a white solid in 59% yield. <sup>1</sup>H NMR (400 MHz, CDCl<sub>3</sub>):  $\delta$  12.10 (s, 1H), 8.29 (s, 1H), 7.95 (d, 1H,  $J$  = 5.9 Hz), 7.53 (dd, 1H,  $J$  = 7.6 Hz, 1.5 Hz), 7.43–7.33 (m, 2H).

**4-(*o*-Tolyl)-1H-1,2,3-triazole (25).**<sup>62</sup> Synthesized from 1-ethynyl-2-methylbenzene<sup>71</sup> and TMSN<sub>3</sub> according to the general procedure to afford **25** as a white solid in 60% yield. <sup>1</sup>H NMR (400 MHz, CDCl<sub>3</sub>):  $\delta$  7.89 (s, 1H), 7.62 (d, 1H,  $J$  = 6.8 Hz), 7.37–7.29 (m, 3H), 2.51 (s, 3H).

**2-(1H-1,2,3-Triazol-4-yl)aniline (26).** Synthesized from 2-ethynylaniline<sup>71</sup> and TMSN<sub>3</sub> according to the general procedure to afford **26** as a white solid in 58% yield, mp 128–130 °C. IR (film):  $\nu$  3377, 3326, 2528, 1483, 1297, 748 cm<sup>-1</sup>. <sup>1</sup>H NMR (400 MHz, CD<sub>3</sub>OD):  $\delta$  8.10 (s, 1H), 7.54 (d, 1H,  $J$  = 7.2 Hz), 7.10 (t, 1H,  $J$  = 7.8 Hz), 6.84 (d, 1H,  $J$  = 7.8 Hz), 6.73 (t, 1H,  $J$  = 7.8 Hz). <sup>13</sup>C NMR (100 MHz, CD<sub>3</sub>OD):  $\delta$  145.1, 128.7, 127.8, 117.3, 116.5, 113.8. ESI-TOF-HRMS:  $m/z$  calcd for (M + H) C<sub>8</sub>H<sub>8</sub>N<sub>4</sub>, 161.0827; found, 161.0834.

**4-(2-Fluorophenyl)-1H-1,2,3-triazole (27).**<sup>121</sup> Synthesized from 1-ethynyl-2-fluorobenzene<sup>71</sup> and TMSN<sub>3</sub> according to the general procedure to afford **27** as a white solid in 52% yield. <sup>1</sup>H NMR (400 MHz, CDCl<sub>3</sub>):  $\delta$  12.24 (s, 1H), 8.19–8.05 (m, 2H), 7.43–7.36 (m, 1H), 7.32–7.26 (m, 1H), 7.25–7.18 (m, 1H).

**4-(2-Ethylphenyl)-1H-1,2,3-triazole (28).** Synthesized from 1-ethyl-2-ethynylbenzene<sup>71</sup> and TMSN<sub>3</sub> according to the general procedure to

afford **28** as yellow oil in 73% yield. IR (film):  $\nu$  3139, 2965, 2931, 2873, 1465, 1443, 968, 761  $\text{cm}^{-1}$ .  $^1\text{H}$  NMR (400 MHz,  $\text{CDCl}_3$ ):  $\delta$  11.70 (br s, 1H), 7.86 (s, 1H), 7.53 (d, 1H,  $J = 7.6$  Hz), 7.42–7.35 (m, 2H), 7.33–7.29 (m, 1H), 2.83 (q, 2H,  $J = 7.5$  Hz), 1.23 (t, 3H,  $J = 7.5$  Hz).  $^{13}\text{C}$  NMR (100 MHz,  $\text{CDCl}_3$ ):  $\delta$  142.6, 129.7, 129.3, 129.1, 128.5, 126.1, 26.6, 15.5. ESI-TOF-HRMS:  $m/z$  calcd for (M + H)  $\text{C}_{10}\text{H}_{11}\text{N}_3$ , 174.1031; found, 174.1039.

**4-(2-(Trifluoromethyl)phenyl)-1H-1,2,3-triazole (29)**.<sup>63</sup> Synthesized from 1-ethynyl-2-(trifluoromethyl)benzene<sup>71</sup> and  $\text{TMSN}_3$  according to the general procedure to afford **29** as a white solid in 46% yield.  $^1\text{H}$  NMR (400 MHz,  $\text{CDCl}_3$ ):  $\delta$  11.83 (s, 1H), 7.94 (s, 1H), 7.83 (d, 1H,  $J = 8.0$  Hz), 7.75 (br s, 1H), 7.67 (t, 1H,  $J = 7.6$  Hz), 7.57 (t, 1H,  $J = 7.7$  Hz).

**2-(1H-1,2,3-Triazol-4-yl)benzaldehyde (30)**. Synthesized from 2-ethynylbenzaldehyde<sup>71</sup> and  $\text{TMSN}_3$  according to the general procedure to afford **30** as a off-white solid in 65% yield, mp 134–137 °C. IR (film):  $\nu$  3132, 3089, 2877, 2168, 1684, 1075, 758  $\text{cm}^{-1}$ .  $^1\text{H}$  NMR (400 MHz,  $\text{CDCl}_3$ ):  $\delta$  12.32 (br s, 1H), 10.40 (s, 1H), 8.09 (d, 1H,  $J = 7.8$  Hz), 8.02 (s, 1H), 7.76–7.69 (m, 2H), 7.63–7.57 (m, 1H).  $^{13}\text{C}$  NMR (100 MHz,  $\text{CD}_3\text{OD}$ ):  $\delta$  192.3, 134.1, 133.6, 130.0, 129.2, 128.5, 128.1, 127.6, 125.9. ESI-TOF-HRMS:  $m/z$  calcd for (M + H)  $\text{C}_9\text{H}_7\text{N}_3\text{O}$ , 174.0667; found, 174.0675.

**N-Methyl-2-(1H-1,2,3-triazol-4-yl)aniline (31)**. Synthesized from 2-ethynyl-N-methylaniline<sup>71</sup> and  $\text{TMSN}_3$  according to the general procedure to afford **31** as a off-white solid in 72% yield, mp 129–131 °C. IR (film):  $\nu$  3405, 3133, 2901, 2268, 1493, 1285, 751  $\text{cm}^{-1}$ .  $^1\text{H}$  NMR (400 MHz,  $\text{CD}_3\text{OD}$ ):  $\delta$  8.11 (s, 1H), 7.56 (d, 1H,  $J = 7.3$  Hz), 7.23 (t, 1H,  $J = 7.7$  Hz), 6.76 (d, 1H,  $J = 8.3$  Hz), 6.71 (t, 1H,  $J = 7.7$  Hz), 2.93 (s, 3H).  $^{13}\text{C}$  NMR (100 MHz,  $\text{CD}_3\text{OD}$ ):  $\delta$  146.8, 129.2, 127.7, 115.6, 113.3, 110.2, 29.4. ESI-TOF-HRMS:  $m/z$  calcd for (M + H)  $\text{C}_9\text{H}_{10}\text{N}_4$ , 175.0984; found, 175.0990.

**4-(2-Methoxyphenyl)-1H-1,2,3-triazole (32)**.<sup>62</sup> Synthesized from 1-ethynyl-2-methoxybenzene<sup>71</sup> and  $\text{TMSN}_3$  according to the general procedure to afford **32** as a white solid in 38% yield.  $^1\text{H}$  NMR (400 MHz,  $\text{CDCl}_3$ ):  $\delta$  12.52 (s, 1H), 8.15 (s, 1H), 7.90 (br s, 1H), 7.43–7.37 (m, 1H), 7.14–7.05 (m, 2H), 4.04 (s, 3H).

**2-(2-(1H-1,2,3-Triazol-4-yl)phenyl)ethanamine Hydrochloride (33)**. Compound **74** (0.20 mmol) was dissolved in diethyl ether (1 mL), and 1 mL of HCl solution (5 N–6 N in isopropyl alcohol)<sup>73</sup> was added dropwise to the stirred solution. The mixture was stirred at ambient temperature for 36 h. The resulting crystals were filtered and washed with diethyl ether to give **33** as a white solid in quantitative yield, mp 202–205 °C, 90% yield. IR (film):  $\nu$  3121, 2897, 2248, 1474, 1142, 763  $\text{cm}^{-1}$ .  $^1\text{H}$  NMR (400 MHz,  $\text{CD}_3\text{OD}$ ):  $\delta$  8.11 (s, 1H), 7.60 (d, 1H,  $J = 6.9$  Hz), 7.47–7.39 (m, 3H), 3.28–3.22 (m, 2H), 3.21–3.16 (m, 2H).  $^{13}\text{C}$  NMR (100 MHz,  $\text{CD}_3\text{OD}$ ):  $\delta$  143.5, 135.3, 130.4, 130.1, 129.8, 127.5, 127.4, 127.3, 40.2, 30.9. ESI-TOF-HRMS:  $m/z$  calcd for (M + H)  $\text{C}_{10}\text{H}_{12}\text{N}_4$ , 189.1140; found, 189.1145.

**3-(2-(1H-1,2,3-Triazol-4-yl)phenyl)propanoic Acid (34)**. The mixture of aldehyde **30** (80 mg, 0.46 mmol) and Meldrum's acid<sup>74</sup> (67 mg, 0.46 mmol) in TEAF (1.0 mL) was stirred at 95–100 °C for 3 h and then cooled to room temperature. Some ice and water (2–3 g) was added to the cold reaction mixture before adjusting its pH to 1 with 6 N HCl (1–2 mL) and letting it crystallize at 5–10 °C for a day. After filtering, the crystals were washed with cold water and pentane to afford **34** as a white solid in 45% yield, mp 119–121 °C. IR (film):  $\nu$  3124, 2857, 1704, 1407, 1212, 975, 765  $\text{cm}^{-1}$ .  $^1\text{H}$  NMR (400 MHz,  $\text{CD}_3\text{OD}$ ):  $\delta$  7.97 (br s, 1H), 7.54–7.47 (m, 1H), 7.41–7.27 (m, 3H), 3.14–3.03 (m, 2H), 2.59–2.51 (m, 2H).  $^{13}\text{C}$  NMR (100 MHz,  $\text{CD}_3\text{OD}$ ):  $\delta$  175.2, 139.0, 129.5, 126.2, 34.8, 28.5. ESI-TOF-HRMS:  $m/z$  calcd for (M + H)  $\text{C}_{11}\text{H}_{11}\text{N}_3\text{O}_2$ , 218.0930; found, 218.0940.

**4-Chloro-2-(1H-1,2,3-triazol-4-yl)phenol (35)**. Synthesized from 4-chloro-2-ethynylphenol<sup>71</sup> and  $\text{TMSN}_3$  according to the general procedure to afford **35** as a off-white solid in 60% yield, mp 212–214 °C. IR (film):  $\nu$  3140, 2923, 2280, 1474, 1230, 813  $\text{cm}^{-1}$ .  $^1\text{H}$  NMR (400 MHz,  $\text{CD}_3\text{OD}$ ):  $\delta$  8.30 (s, 1H), 7.90 (s, 1H), 7.20 (dd, 1H,  $J = 7.1$  Hz, 2.5 Hz), 6.92 (d, 1H,  $J = 8.8$  Hz).  $^{13}\text{C}$  NMR (100 MHz,  $\text{CD}_3\text{OD}$ ):  $\delta$  153.3, 128.6, 126.3, 124.1, 117.3. ESI-TOF-HRMS:  $m/z$  calcd for (M + H)  $\text{C}_8\text{H}_6\text{ClN}_3\text{O}$ , 196.0278; found, 196.0277.

**4-(5-Chloro-2-methylphenyl)-1H-1,2,3-triazole (36)**. Synthesized from 4-chloro-2-ethynyl-1-methylbenzene<sup>71</sup> and  $\text{TMSN}_3$  according to the general procedure to afford **36** as a white solid in 52% yield, mp 122–124 °C. IR (film):  $\nu$  3091, 2869, 2752, 2604, 1480, 1074, 880, 802  $\text{cm}^{-1}$ .  $^1\text{H}$  NMR (400 MHz,  $\text{CDCl}_3\text{-CD}_3\text{OD}$ ):  $\delta$  7.80 (s, 1H), 7.60 (br s, 1H), 7.25–7.16 (m, 2H), 2.40 (s, 3H).  $^{13}\text{C}$  NMR (100 MHz,  $\text{CD}_3\text{OD}$ ):  $\delta$  134.5, 132.1, 131.3, 128.2, 127.8, 19.5. ESI-TOF-HRMS:  $m/z$  calcd for (M + H)  $\text{C}_9\text{H}_8\text{ClN}_3$ , 194.0485; found, 194.0480.

**4-(2,5-Dichlorophenyl)-1H-1,2,3-triazole (37)**. Synthesized from 1,4-dichloro-2-ethynylbenzene<sup>71</sup> and  $\text{TMSN}_3$  according to the general procedure to afford **37** as a white solid in 70% yield, mp 175–176 °C. IR (film):  $\nu$  3161, 3061, 2095, 1466, 1054, 803  $\text{cm}^{-1}$ .  $^1\text{H}$  NMR (400 MHz,  $\text{CDCl}_3\text{-CD}_3\text{OD}$ ):  $\delta$  8.35 (s, 1H), 7.96 (s, 1H), 7.49 (d, 1H,  $J = 8.6$  Hz), 7.35 (dd, 1H,  $J = 7.3$  Hz, 2.3 Hz).  $^{13}\text{C}$  NMR (100 MHz,  $\text{CD}_3\text{OD}$ ):  $\delta$  142.1, 132.7, 131.4, 130.7, 129.9, 129.3, 129.0. ESI-TOF-HRMS:  $m/z$  calcd for (M + H)  $\text{C}_8\text{H}_5\text{F}_3\text{Cl}_2\text{N}_3$ , 213.9939; found, 213.9945.

**4-(2,3-Dichlorophenyl)-1H-1,2,3-triazole (38)**. Synthesized from 1,2-dichloro-3-ethynylbenzene<sup>71</sup> and  $\text{TMSN}_3$  according to the general procedure to afford **38** as a white solid in 71% yield, mp 168–170 °C. IR (film):  $\nu$  3170, 3071, 2642, 2112, 1444, 1073, 779  $\text{cm}^{-1}$ .  $^1\text{H}$  NMR (400 MHz,  $\text{CD}_3\text{OD}$ ):  $\delta$  8.32 (s, 1H), 7.83 (d, 1H,  $J = 7.7$  Hz), 7.56 (d, 1H,  $J = 7.7$  Hz), 7.38 (t, 1H,  $J = 7.7$  Hz).  $^{13}\text{C}$  NMR (100 MHz,  $\text{CD}_3\text{OD}$ ):  $\delta$  142.6, 133.5, 131.5, 129.9, 128.5, 127.6. ESI-TOF-HRMS:  $m/z$  calcd for (M + H)  $\text{C}_8\text{H}_5\text{Cl}_2\text{N}_3$ , 213.9939; found, 213.9933.

**4-(3-Chloro-2-methylphenyl)-1H-1,2,3-triazole (39)**. Synthesized from 1-chloro-3-ethynyl-2-methylbenzene<sup>71</sup> and  $\text{TMSN}_3$  according to the general procedure to afford **39** as a white solid in 51% yield, mp 135–137 °C. IR (film):  $\nu$  3162, 2907, 2139, 1572, 1438, 1067, 801  $\text{cm}^{-1}$ .  $^1\text{H}$  NMR (400 MHz,  $\text{CDCl}_3\text{-CD}_3\text{OD}$ ):  $\delta$  7.80 (s, 1H), 7.44–7.38 (m, 2H), 7.20 (t, 1H,  $J = 7.9$  Hz).  $^{13}\text{C}$  NMR (100 MHz,  $\text{CD}_3\text{OD}$ ):  $\delta$  135.1, 134.1, 132.8, 129.1, 128.0, 126.6, 16.5. ESI-TOF-HRMS:  $m/z$  calcd for (M + H)  $\text{C}_9\text{H}_8\text{ClN}_3$ , 194.0485; found, 194.0494.

**3-Methyl-2-(1H-1,2,3-triazol-4-yl)aniline (40)**. To a solution of **41** (40 mg, 0.15 mmol) in dioxane (2 mL),  $\text{N}_2\text{H}_4\cdot\text{H}_2\text{O}$ <sup>75</sup> (38 mg, 0.75 mmol) was added dropwise at room temperature. The mixture was refluxed for 2.5 h, cooled to room temperature, filtered, and evaporated. The residue was dissolved in  $\text{CH}_2\text{Cl}_2$  (5 mL), and the solution was washed with brine (2 × 4 mL) and dried over  $\text{Na}_2\text{SO}_4$ . Evaporation gave **40** as a white solid in 50% yield, mp 146–148 °C. IR (film):  $\nu$  3354, 3123, 2922, 1583, 1466, 962, 771  $\text{cm}^{-1}$ .  $^1\text{H}$  NMR (400 MHz,  $\text{CDCl}_3$ ):  $\delta$  7.82 (s, 1H), 7.13 (t, 1H,  $J = 7.8$  Hz), 6.74 (d, 1H,  $J = 7.4$  Hz), 6.70 (d, 1H,  $J = 8.0$  Hz), 2.21 (s, 3H).  $^{13}\text{C}$  NMR (100 MHz,  $\text{CD}_3\text{OD}$ ):  $\delta$  146.3, 137.8, 129.2, 119.5, 113.4, 19.4. ESI-TOF-HRMS:  $m/z$  calcd for (M + H)  $\text{C}_9\text{H}_{10}\text{N}_4$ , 175.0984; found, 175.0978.

**2,2,2-Trifluoro-N-(3-methyl-2-(1H-1,2,3-triazol-4-yl)phenyl)acetamide (41)**. Synthesized from N-(2-ethynyl-3-methylphenyl)-2,2,2-trifluoroacetamide<sup>71</sup> and  $\text{TMSN}_3$  according to the general procedure to afford **41** as a white solid in 45% yield, mp 181–183 °C. IR (film):  $\nu$  3162, 2938 1698, 1555, 1458, 1213, 1184, 1135, 1066, 771  $\text{cm}^{-1}$ .  $^1\text{H}$  NMR (400 MHz,  $\text{CD}_3\text{OD}$ ):  $\delta$  7.90 (s, 1H), 7.53 (d, 1H,  $J = 7.7$  Hz), 7.40 (t, 1H,  $J = 7.7$  Hz), 7.33 (d, 1H,  $J = 7.7$  Hz), 2.30 (s, 3H).  $^{13}\text{C}$  NMR (100 MHz,  $\text{CD}_3\text{OD}$ ):  $\delta$  156.0 (q,  $J = 40.1$ ), 138.7, 133.8, 129.1, 128.9, 125.3, 122.9, 116.0, (q,  $J = 287.5$ ), 19.7. ESI-TOF-HRMS:  $m/z$  calcd for (M + H)  $\text{C}_{11}\text{H}_9\text{F}_3\text{N}_4\text{O}$ , 271.0807; found, 271.0808.

**4-Methyl-3-(1H-1,2,3-triazol-4-yl)aniline (42)**. Synthesized from 3-ethynyl-4-methylaniline<sup>71</sup> and  $\text{TMSN}_3$  according to the general procedure to afford **42** as yellow semisolid in 40% yield. IR (film):  $\nu$  3349, 3136, 2925, 1619, 1493, 1242, 1124, 817  $\text{cm}^{-1}$ .  $^1\text{H}$  NMR (400 MHz,  $\text{CD}_3\text{OD}$ ):  $\delta$  7.86 (s, 1H), 7.11 (d, 1H,  $J = 8.1$  Hz), 7.0 (d, 1H,  $J = 2.4$  Hz), 6.69 (dd, 1H,  $J = 5.6$  Hz, 2.5 Hz), 2.38 (s, 3H).  $^{13}\text{C}$  NMR (100 MHz,  $\text{CD}_3\text{OD}$ ):  $\delta$  144.6, 131.3, 128.6, 125.6, 116.2, 116.0, 18.8. ESI-TOF-HRMS:  $m/z$  calcd for (M + H)  $\text{C}_9\text{H}_{10}\text{N}_4$ , 175.0984; found, 175.0980.

**1,5-Diphenyl-1H-1,2,3-triazole (43)**.<sup>80,81</sup> To a solution of EtMgBr in THF (1.0 M, 2 mL), phenylacetylene (0.22 mL, 2 mmol) was added at room temperature. The reaction mixture was heated to 50 °C for 15

min. After cooling the mixture to room temperature, a solution of phenylazide (0.24 g, 2 mmol) in THF (0.8 mL) was added. The resulting solution was stirred at room temperature for 30 min and then heated to 50 °C for 1 h before quenching with saturated NH<sub>4</sub>Cl (2 mL). The layers were separated, and the aqueous layer was extracted with CH<sub>2</sub>Cl<sub>2</sub> (3 × 3 mL). The combined organic layers were dried over Na<sub>2</sub>SO<sub>4</sub> and concentrated under reduced pressure. The residue was purified by flash column chromatography on silica gel to afford **43** as a white solid in 60% yield. <sup>1</sup>H NMR (400 MHz, CDCl<sub>3</sub>): δ 7.89 (s, 1H), 7.48–7.44 (m, 3H), 7.42–7.35 (m, 5H), 7.27–7.24 (m, 2H).

**5-(4-Fluorophenyl)-1-phenyl-1H-1,2,3-triazole (44)**. Using the same procedure<sup>80,81</sup> as that used for **43**, starting from 1-ethynyl-4-fluorobenzene (115 mg, 1 mmol) in the presence of a solution of EtMgBr (1.0 M, 1 mL), product **44** was obtained as a white solid in 55% yield, mp 100–103 °C. IR (film): ν 3122, 1893, 1492, 1229, 1160, 830, 768 cm<sup>-1</sup>. <sup>1</sup>H NMR (400 MHz, CD<sub>3</sub>OD): δ 7.97 (s, 1H), 7.54–7.47 (m, 3H), 7.39–7.35 (m, 2H), 7.33–7.28 (m, 2H), 7.13–7.07 (m, 2H). <sup>13</sup>C NMR (100 MHz, CD<sub>3</sub>OD): δ 163.3 (d, J = 249.7 Hz), 137.5, 136.3, 132.7, 130.7 (d, J = 8.7 Hz), 129.5, 129.3, 125.4, 122.6 (d, J = 3.6 Hz), 115.6 (d, J = 22.4 Hz). ESI-TOF-HRMS: *m/z* calcd for (M + H) C<sub>14</sub>H<sub>10</sub>FN<sub>3</sub>, 240.0937; found, 240.0931.

**1-Phenyl-5-(*m*-tolyl)-1H-1,2,3-triazole (45)**. Using the same procedure<sup>80,81</sup> as that used for **43**, starting from 1-ethynyl-3-methylbenzene (116 mg, 1 mmol) in the presence of a solution of EtMgBr (1.0 M, 1 mL), product **45** was obtained as a white solid in 35% yield, mp 109–113 °C. IR (film): ν 2920, 1597, 1499, 1456, 1234, 1050, 763 cm<sup>-1</sup>. <sup>1</sup>H NMR (400 MHz, CD<sub>3</sub>OD): δ 7.97 (s, 1H), 7.56–7.48 (m, 3H), 7.41–7.36 (m, 2H), 7.25–7.20 (m, 2H), 7.14 (br s, 1H), 7.06–7.01 (m, 1H), 2.28 (s, 3H). <sup>13</sup>C NMR (100 MHz, CD<sub>3</sub>OD): δ 138.7, 138.6, 136.5, 132.5, 129.8, 129.4, 129.2, 128.9, 128.4, 126.2, 125.5, 125.3, 19.8. ESI-TOF-HRMS: *m/z* calcd for (M + H) C<sub>15</sub>H<sub>13</sub>N<sub>3</sub>, 236.1188; found, 236.1184.

**5-(3-Chlorophenyl)-1-phenyl-1H-1,2,3-triazole (46)**. Using the same procedure<sup>80,81</sup> as that used for **43**, starting from 1-chloro-3-ethynylbenzene (123 mg, 1 mmol) in the presence of a solution of EtMgBr (1.0 M, 1 mL), product **46** was obtained as a white solid in 70% yield, mp 85–87 °C. IR (film): ν 2920, 1597, 1499, 1456, 1234, 1050, 763 cm<sup>-1</sup>. <sup>1</sup>H NMR (400 MHz, CD<sub>3</sub>OD): δ 8.01 (s, 1H), 7.55–7.47 (m, 3H), 7.40–7.35 (m, 3H), 7.34–7.29 (m, 2H), 7.19–7.15 (m, 1H). <sup>13</sup>C NMR (100 MHz, CD<sub>3</sub>OD): δ 137.0, 136.2, 134.4, 133.0, 130.1, 129.7, 129.4, 129.1, 128.3, 126.9, 125.4. ESI-TOF-HRMS: *m/z* calcd for (M + H) C<sub>14</sub>H<sub>10</sub>ClN<sub>3</sub>, 256.0641; found, 256.0644.

**5-(2-Methoxyphenyl)-1-phenyl-1H-1,2,3-triazole (47)**.<sup>80,81</sup> Using the same procedure<sup>80,81</sup> as that used for **43**, starting from 1-ethynyl-2-methoxybenzene (131 mg, 1 mmol) in the presence of a solution of EtMgBr (1.0 M, 1 mL), product **47** was obtained as a white solid in 50% yield. <sup>1</sup>H NMR (400 MHz, CDCl<sub>3</sub>): δ 7.85 (s, 1H), 7.44–7.33 (m, 5H), 7.28–7.24 (m, 2H), 7.01 (td, 1H, J = 7.5 Hz, 1.0 Hz), 6.86 (d, 1H, J = 8.4 Hz), 3.44 (s, 3H).

**1-Methyl-5-phenyl-1H-1,2,3-triazole (48)**.<sup>83,84</sup> Synthesized from 4-phenyl-1H-1,2,3-triazole and dimethyl carbonate according to the general procedure of *N*-alkylation<sup>82</sup> to afford **48** as a light yellow oil, 7% yield. <sup>1</sup>H NMR (400 MHz, CDCl<sub>3</sub>): δ 7.75 (s, 1H), 7.56–7.49 (m, 3H), 7.46–7.43 (m, 2H), 4.11 (s, 3H).

**1-Methyl-4-phenyl-1H-1,2,3-triazole (49)**.<sup>83,84</sup> Synthesized from 4-phenyl-1H-1,2,3-triazole and dimethyl carbonate according to the general procedure of *N*-alkylation<sup>82</sup> to afford **49** as a white solid, 50% yield. <sup>1</sup>H NMR (400 MHz, CDCl<sub>3</sub>): δ 7.86–7.83 (m, 2H), 7.77 (s, 1H), 7.47–7.43 (m, 2H), 7.38–7.33 (m, 1H), 4.18 (s, 3H).

**2-Methyl-4-phenyl-2H-1,2,3-triazole (50)**.<sup>83,84</sup> Synthesized from 4-phenyl-1H-1,2,3-triazole and dimethyl carbonate according to the general procedure of *N*-alkylation<sup>82</sup> to afford **50** as a white solid, 20% yield. <sup>1</sup>H NMR (400 MHz, CDCl<sub>3</sub>): δ 7.85 (s, 1H), 7.80 (d, 2H, J = 7.5 Hz), 7.45 (t, 2H, J = 7.5 Hz), 7.40–7.35 (m, 1H), 4.27 (s, 3H).

**1-Ethyl-5-phenyl-1H-1,2,3-triazole (51)**.<sup>86</sup> Synthesized from 4-phenyl-1H-1,2,3-triazole and diethyl carbonate according to the general procedure of *N*-alkylation<sup>82</sup> to afford **51** as a yellow oil, 6% yield. <sup>1</sup>H NMR (400 MHz, CDCl<sub>3</sub>): δ 7.72 (s, 1H), 7.56–7.48 (m, 3H), 7.44–7.39 (m, 2H), 4.43 (q, 2H, J = 7.3 Hz), 1.51 (t, 3H, J = 7.3 Hz).

**2-Ethyl-4-phenyl-2H-1,2,3-triazole (52)**.<sup>86</sup> Synthesized from 4-phenyl-1H-1,2,3-triazole and diethyl carbonate according to the general procedure of *N*-alkylation<sup>82</sup> to afford **51** as a colorless oil, 19% yield. <sup>1</sup>H NMR (400 MHz, CDCl<sub>3</sub>): δ 7.85 (s, 1H), 7.81 (d, 2H, J = 7.5 Hz), 7.45 (t, 2H, J = 7.5 Hz), 7.40–7.34 (m, 1H), 4.54 (q, 2H, J = 7.3 Hz), 1.63 (t, 3H, J = 7.4 Hz).

**1-Ethyl-4-phenyl-1H-1,2,3-triazole (53)**.<sup>86</sup> Synthesized from 4-phenyl-1H-1,2,3-triazole and diethyl carbonate according to the general procedure of *N*-alkylation<sup>82</sup> to afford **52** as a white solid, 55% yield. <sup>1</sup>H NMR (400 MHz, CDCl<sub>3</sub>): δ 7.86 (d, 2H, J = 7.5 Hz), 7.78 (s, 1H), 7.45 (t, 2H, J = 7.6 Hz), 7.36 (t, 1H, J = 7.5 Hz), 4.49 (q, 2H, J = 7.4 Hz), 1.67 (t, 3H, J = 7.4 Hz).

**1-Butyl-5-phenyl-1H-1,2,3-triazole (54)**.<sup>78,79</sup> Synthesized according to a previously reported procedure.<sup>78,79</sup> Oil, 13% yield. <sup>1</sup>H NMR (400 MHz, CDCl<sub>3</sub>): δ 7.71 (s, 1H), 7.55–7.49 (m, 3H), 7.42–7.39 (m, 2H), 4.37 (t, 2H, J = 7.4 Hz), 1.84 (quintet, 2H, J = 7.4 Hz), 1.30 (sextet, 2H, J = 7.5 Hz), 0.88 (t, 3H, J = 7.4 Hz).

**1-Butyl-4-phenyl-1H-1,2,3-triazole (55)**.<sup>78,79</sup> Synthesized according to a previously reported procedure.<sup>78,79</sup> White solid, 40% yield. <sup>1</sup>H NMR (400 MHz, CDCl<sub>3</sub>): δ 7.88–7.84 (m, 2H), 7.77 (s, 1H), 7.48–7.42 (m, 2H), 7.38–7.33 (m, 1H), 4.44 (t, 2H, J = 7.5 Hz), 1.97 (quintet, 2H, J = 7.5 Hz), 1.43 (sextet, 2H, J = 7.6 Hz), 1.0 (t, 3H, J = 7.5 Hz).

**1-Benzyl-5-phenyl-1H-1,2,3-triazole (56)**.<sup>78,79</sup> Synthesized according to a previously reported procedure.<sup>78,79</sup> Off-white solid, 15% yield. <sup>1</sup>H NMR (400 MHz, CDCl<sub>3</sub>): δ 7.77 (s, 1H), 7.48–7.41 (m, 3H), 7.35–7.25 (m, 5H), 7.13–7.08 (m, 2H), 5.58 (s, 2H).

**1-Benzyl-4-phenyl-1H-1,2,3-triazole (57)**.<sup>78,79</sup> Synthesized according to a previously reported procedure.<sup>78,79</sup> White solid, 45% yield. <sup>1</sup>H NMR (400 MHz, CDCl<sub>3</sub>): δ 7.85–7.80 (m, 2H), 7.68 (s, 1H), 7.45–7.38 (m, 5H), 7.37–7.31 (m, 3H), 5.61 (s, 2H).

**4-Methyl-5-phenyl-1H-1,2,3-triazole (58)**.<sup>76</sup> Synthesized according to a previously reported procedure.<sup>76</sup> White solid, 30% yield. <sup>1</sup>H NMR (400 MHz, CDCl<sub>3</sub>): δ 11.53 (s, 1H), 7.74 (d, 2H, J = 7.7 Hz), 7.52–7.47 (m, 2H), 7.44–7.39 (m, 1H), 2.57 (s, 3H).

**5-(3-Chlorophenyl)-1-methyl-1H-1,2,3-triazole (59)**. Synthesized from **8** and iodomethane according to the general procedure of *N*-methylation<sup>82</sup> to afford **59** as a yellow oil, 7% yield. IR (film): ν 2926, 2854, 1732, 1571, 1473, 1454, 1245, 1098, 790 cm<sup>-1</sup>. <sup>1</sup>H NMR (400 MHz, CD<sub>3</sub>OD): δ 7.86 (s, 1H), 7.64–7.62 (m, 1H), 7.56–7.49 (m, 3H), 4.12 (s, 3H). <sup>13</sup>C NMR (100 MHz, CD<sub>3</sub>OD): δ 136.0, 133.7, 131.7, 130.6, 129.8, 129.6, 128.1, 30.6. ESI-TOF-HRMS: *m/z* calcd for (M + H) C<sub>9</sub>H<sub>8</sub>ClN<sub>3</sub>, 194.0485; found, 194.0478.

**4-(3-Chlorophenyl)-1-methyl-1H-1,2,3-triazole (60)**. Synthesized from **8** and iodomethane according to the general procedure of *N*-methylation<sup>82</sup> to afford **60** as a white solid, mp 104–107 °C, 49% yield. IR (film): ν 3142, 2949, 2158, 1421, 1078, 887 cm<sup>-1</sup>. <sup>1</sup>H NMR (400 MHz, CD<sub>3</sub>OD): δ 8.26 (s, 1H), 7.80 (br s, 1H), 7.69 (d, 1H, J = 7.7 Hz), 7.38 (t, 1H, J = 7.9 Hz), 7.31 (br d, 1H, J = 7.9 Hz), 4.13 (s, 3H). <sup>13</sup>C NMR (100 MHz, CD<sub>3</sub>OD): δ 146.1, 134.5, 132.4, 130.2, 127.7, 125.0, 123.5, 122.3, 35.7. ESI-TOF-HRMS: *m/z* calcd for (M + H) C<sub>9</sub>H<sub>8</sub>ClN<sub>3</sub>, 194.0485; found, 194.0484.

**1-Phenyl-1H-1,2,3-triazole (61)**.<sup>77</sup> Synthesized according to a previously reported procedure.<sup>77</sup> Off-white solid, 71% yield. <sup>1</sup>H NMR (400 MHz, CDCl<sub>3</sub>): δ 8.02 (d, 1H, J = 1.0 Hz), 7.88 (d, 1H, J = 1.0 Hz), 7.80–7.76 (m, 2H), 7.59–7.54 (m, 2H), 7.50–7.45 (m, 1H).

**4-Benzyl-1H-1,2,3-triazole (62)**.<sup>128</sup> Synthesized from prop-2-yn-1-ylbenzene<sup>71</sup> and TMSN<sub>3</sub> according to the general procedure to afford **62** as a light-yellow solid in 45% yield. <sup>1</sup>H NMR (400 MHz, CDCl<sub>3</sub>): δ 11.78 (s, 1H), 7.48 (s, 1H), 7.37–7.31 (m, 2H), 7.30–7.24 (m, 3H), 4.13 (s, 2H).

**4-((Phenylthio)methyl)-1H-1,2,3-triazole (63)**.<sup>120</sup> Synthesized from phenyl(prop-2-yn-1-yl)sulfane<sup>71</sup> and TMSN<sub>3</sub> according to the general procedure to afford **63** as an off-white solid in 55% yield. <sup>1</sup>H NMR (400 MHz, CDCl<sub>3</sub>): δ 11.73 (s, 1H), 7.57 (s, 1H), 7.40–7.35 (m, 2H), 7.33–7.27 (m, 2H), 7.26–7.22 (m, 1H), 4.25 (s, 2H).

**4-(Cyclohex-1-en-1-yl)-1H-1,2,3-triazole (64)**.<sup>129</sup> Synthesized from 1-ethynylcyclohex-1-ene<sup>71</sup> and TMSN<sub>3</sub> according to the general procedure to afford **64** as a white solid in 65% yield. <sup>1</sup>H NMR (400 MHz, CDCl<sub>3</sub>): δ 11.65 (s, 1H), 7.70 (s, 1H), 6.43 (br s, 1H), 2.51–



2.44 (m, 2H), 2.28–2.21 (m, 2H), 1.85–1.77 (m, 2H), 1.76–1.67 (m, 2H).

**tert-Butyl N-[2-[2-(1H-1,2,3-Triazol-4-yl)phenyl]ethyl]carbamate (74).** Synthesized from *tert*-butyl 2-ethynylphenethylcarbamate<sup>71</sup> and TMSN<sub>3</sub> according to the general procedure to afford 74 as yellow oil in 45% yield. IR (film):  $\nu$  3137, 2977, 2932, 1681, 1514, 1366, 1167, 765 cm<sup>-1</sup>. <sup>1</sup>H NMR (400 MHz, CDCl<sub>3</sub>):  $\delta$  7.90 (s, 1H), 7.56–7.52 (m, 1H), 7.42–7.31 (m, 3H), 4.98 (br s, 1H) 3.40 (q, 2H,  $J$  = 6.8 Hz), 2.99 (t, 2H,  $J$  = 7.1 Hz), 1.45 (s, 9H). <sup>13</sup>C NMR (100 MHz, CDCl<sub>3</sub>):  $\delta$  156.7, 137.2, 130.8, 129.9, 128.8, 126.8, 79.7, 41.8, 34.0, 28.5. ESI-TOF-HRMS:  $m/z$  calcd for (M + H) C<sub>15</sub>H<sub>20</sub>N<sub>4</sub>O<sub>2</sub>, 289.1664; found, 289.1655.

**Protein Expression and Purification of Recombinant Human IDO1.** The coding region for human IDO1 (Ala2-Gly403) was cloned into a derivative of plasmid pET9 (Novagen). The recombinant plasmid, pETIDO, encodes a histidine tag at the N-terminus of IDO1. The bacterial strain BL21 AI (Invitrogen) was used for overexpression of IDO1 and transformed with the plasmid pETIDO. The transformed cells were grown on a rotary shaker at 37 °C and 220 rpm to an OD<sub>600</sub> of 1.2, in LB medium supplemented with kanamycin 25  $\mu$ g/mL, *L*-tryptophan 50  $\mu$ g/mL, and bovine hemin (Sigma) 10  $\mu$ M. The culture was cooled in a water/ice bath and supplemented again with *L*-tryptophan 50  $\mu$ g/mL, bovine hemin 10  $\mu$ M. The expression of histagged IDO1 was induced by the addition of 1% (w/v) arabinose. Induced cells were grown at 20 °C, 60 rpm for 20 h. Cells (1 L culture) were collected by centrifugation, resuspended in 40 mL of Mes 25 mM, KCl 150 mM, imidazole 10 mM, protease inhibitors (complete EDTA free, Roche Applied Science), pH 6.5, and disrupted with a French press. The extract was clarified by centrifugation and filtration on a 0.22  $\mu$ m filter. The enzyme was purified by IMAC using Ni<sup>2+</sup> as ligand and an IMAC HITRAP column (5 mL; GE Healthcare). Briefly, the extract was loaded on the column with buffer Mes 25 mM, KCl 150 mM, imidazole 10 mM, pH 6.5. The column was washed with 50 mL of the same buffer with imidazole adjusted to 100 mM. Finally, the protein was eluted with Mes 25 mM, KCl 150 mM, EDTA 50 mM, pH 6.5. The buffer was then exchanged to Mes 25 mM, KCl 150 mM, pH 6.5 using a HITRAP desalting column (GE Healthcare). The purity of the enzyme was estimated to be >95% based on SDS PAGE gel and Coomassie blue staining. The ratio of absorbance 404 nm/280 nm of the protein was around 1.9.

**Enzymatic Assay.** The enzymatic inhibition assays were performed as described by Takikawa et al.<sup>130</sup> with some modifications. Briefly, the reaction mixture (100  $\mu$ L) contained potassium phosphate buffer (100 mM, pH 6.5) ascorbic acid (20 mM), catalase (400 units/mL), methylene blue (10  $\mu$ M), purified recombinant IDO1 (2.5 ng/ $\mu$ L), *L*-Trp (100  $\mu$ M), and DMSO (5  $\mu$ L). The inhibitors were serially diluted 10-fold from 1000 to 0.1  $\mu$ M, or, if not soluble at 1000  $\mu$ M, by 4 orders of magnitude from their highest soluble concentration. The reaction was carried out at ambient temperature for 60 min and stopped by addition of 30% (w/v) trichloroacetic acid (40  $\mu$ L). To convert *N*-formylkynurenine to kynurenine, the samples were incubated at 50 °C for 30 min, followed by centrifugation at 2500g for 20 min. Lastly, 100  $\mu$ L of supernatant from each probe was used for HPLC analysis. The mobile phase for HPLC measurements consisted of 50% sodium citrate buffer (40 mM, pH 2.35) and 50% methanol with 400  $\mu$ M SDS. The flow rate through the SS-ODS1 column was 1 mL/min, and kynurenine was detected at a wavelength of 365 nm. A compound was defined to be “inactive” if it did not show a clear signal on the dose–response curve, typically at a maximal concentration of 1 mM.

**Cellular Assay. Cell Lines.** For the assay evaluating inhibition of murine IDO1 and murine TDO, we used cell lines P815-mIDO1 clone 6 and P815-mTDO clone 12, respectively, as described in Röhrig et al.<sup>53</sup> For human IDO1, we transfected mouse mastocytoma line P815B with a plasmid construct encoding human IDO1 and selected clone P815B-hIDO1 clone 6, which we used in the assay. For human TDO, we transfected mouse mastocytoma line P815B with a plasmid construct encoding human TDO and selected clone P815B-hTDO clone 19, which overexpressed hTDO and was used in the cellular assay. To estimate cytotoxicity (LD<sub>50</sub>), we used Hep G2 cells.

**Assay.** The assay was performed in 96-well flat bottom plates seeded with  $2 \times 10^5$  cells in a final volume of 200  $\mu$ L of IMDM (Iscove's Modified Dulbecco's Medium, Invitrogen) (80  $\mu$ M *L*-tryptophan) supplemented with 2% FCS and a titration of the compound ranging from 0.001 to 100  $\mu$ M. The cells were incubated at 37 °C. Kynurenine production in control wells without inhibitor was monitored periodically during the assay using 4-(dimethylamino)-benzaldehyde (pDMAB) as described below. The reaction was stopped before 50% of the initial amount of tryptophan was converted into kynurenine to ensure linearity of the reaction. The plates were then centrifuged for 10 min at 300g, and 150  $\mu$ L of the supernatant were collected for HPLC analysis of tryptophan and kynurenine concentrations. Proteins were precipitated by mixing 50  $\mu$ L of supernatant with an equal volume of TCA 6%. After centrifugation, 70  $\mu$ L of supernatant were collected, diluted in an equal volume of water, and injected into the HPLC system (C18 column). Tryptophan was detected at an absorption wavelength of 280 nm and kynurenine at 360 nm.

To measure kynurenine production during the assay, 200  $\mu$ L of supernatant from control wells were mixed with 40  $\mu$ L TCA 30% and centrifuged at 3000g for 5 min. Then 100  $\mu$ L of supernatant were mixed with an equal amount of pDMAB 2% in acetic acid and incubated for 10 min at room temperature. Kynurenine concentration was determined by measuring absorbance at 480 nm. A standard curve was made with pure kynurenine (ICN Biochemicals).

To estimate cytotoxicity (LD<sub>50</sub>),  $2 \times 10^4$  Hep G2 cells were plated in 96-well flat bottom plates in a final volume of 200  $\mu$ L of IMDM (Invitrogen) supplemented with 10% FCS and a titration of the compound ranging from 0.001 to 100  $\mu$ M. After 24 h of incubation at 37 °C, the number of living cells was evaluated with a MTS/PMS assay (Promega) as described by the manufacturer.

**Determination of pK<sub>a</sub> Values.** pK<sub>a</sub> values were determined spectroscopically.<sup>131</sup> About 1 mg of triazole compound were dissolved in 100 mL of water under strong agitation and sonication. Then 75 mg of KCl were added to keep the ionic strength weak but approximately constant (10 mM). The filtered solution was brought to pH 2–3 by addition of few drops of 1 M HCl. Then 300  $\mu$ L were transferred to a Greiner UV-Star 96-well plate, and its absorption spectra was recorded immediately in 1 nm steps between 230 and 350 nm on a Tecan Safire2 microplate reader. A few drops of 1 M NaOH were added to bring the bulk solution to pH 11–12, and another sample of 300  $\mu$ L was transferred to the plate for an absorbance scan. If the spectra allowed to differentiate between different species, in the following the pH was varied in the region of the expected pK<sub>a</sub> values  $\pm 1$  pH unit in steps of roughly 0.2 pH units by addition of a few drops of a diluted HCl solution. At each step, a spectra was measured in above-mentioned wavelength interval. As no buffer was used, care was taken to measure the spectra immediately after stabilization of the pH in order to avoid pH drifts due to the dissolution of CO<sub>2</sub>. The wavelengths with the largest change in optical density  $A$  at different pH values were chosen for analysis and fitted with the function

$$\text{pH} = \text{pK}_a + \log \frac{A - A_1}{A_M - A} \quad (5)$$

where  $A_1$  is the absorbance of the ionized species, and  $A_M$  is the absorbance of the molecular species. As the pK<sub>a</sub> values of the phenol moiety present in some compounds differs by more than 1.6 pK<sub>a</sub> units from the pK<sub>a</sub> values of the triazole moiety, and as both moieties give rise to different absorption peaks, these pK<sub>a</sub> values could be determined independently.

**UV Spectra.** UV spectra were recorded on a Tecan Safire2 microplate reader with 10  $\mu$ M IDO1 in 100 mM phosphate buffer (pH 6.5) and 5% DMSO at room temperature.

## ■ ASSOCIATED CONTENT

### Supporting Information

Figures of possible binding modes of selected compounds to heme, ligand–heme binding energies calculated with DFT, the values of the terms entering into the QSAR model, results of

the elemental analysis for compounds **12**, **18**, **19**, **20**, **21**, **26**, **28**, **30**, **31**, **35**, **36**, **37**, **38**, **39**, **41**, **44**, **46**, and **60**, and dose–response curves of all active compounds in the enzymatic assay. This material is available free of charge via the Internet at <http://pubs.acs.org>.

## AUTHOR INFORMATION

### Corresponding Author

\*For V.Z.: E-mail, [vincent.zoete@isb-sib.ch](mailto:vincent.zoete@isb-sib.ch). Phone, +41-21-692 4082. Fax, +41-21-692 4065. For O.M.: E-mail, [olivier.michielin@isb-sib.ch](mailto:olivier.michielin@isb-sib.ch); Phone, +41-21-692 4053. Fax, +41-21-692 4065.

### Author Contributions

#Both authors contributed equally to this work (U.F.R. and S.R.M.).

### Notes

The authors declare no competing financial interest.

## ACKNOWLEDGMENTS

We are much obliged to the Center of Integrative Genomics (University of Lausanne), especially to Gilles Boss, for assistance with the enzymatic assay. For computational resources and support, we thank the Vital-IT team at the Swiss Institute for Bioinformatics and the Computing services at the University of Lausanne, especially Hamid Hussain-Khan. This work was supported by the Clinical Discovery Program of the Ludwig Institute for Cancer Research, by fund 310030-130857 to O.M. and V.Z. from the Swiss National Science Foundation, and by CANTOL, a project of BioWin, the Health Cluster of Wallonia (Belgium). Molecular graphics and analyses were performed with the UCSF Chimera package from the Resource for Biocomputing, Visualization, and Informatics at the University of California, San Francisco, with support from the National Institutes of Health (National Center for Research Resources grant 2P41RR001081, National Institute of General Medical Sciences grant 9P41GM103311).<sup>132</sup> Instant JChem was used for structure database management, search, and prediction, Instant JChem 5.9, 2012, ChemAxon (<http://www.chemaxon.com>). Marvin was used for drawing, displaying, and characterizing chemical structures, Marvin 5.5, 2011, ChemAxon (<http://www.chemaxon.com>).

## ABBREVIATIONS USED

IDO1, indoleamine 2,3-dioxygenase 1; BM, binding mode; MMBP, Morse-like metal binding potential; PCM, polarizable continuum model; PIM, 4-phenylimidazole; TDO, tryptophan 2,3-dioxygenase

## REFERENCES

- (1) Du, C.; Wang, Y. The immunoregulatory mechanisms of carcinoma for its survival and development. *J. Exp. Clin. Cancer Res.* **2011**, *30*, 12.
- (2) Zamanakou, M.; Germenis, A. E.; Karanikas, V. Tumor immune escape mediated by indoleamine 2,3-dioxygenase. *Immunol. Lett.* **2007**, *111*, 69–75.
- (3) Katz, J. B.; Muller, A. J.; Prendergast, G. C. Indoleamine 2,3-dioxygenase in T-cell tolerance and tumoral immune escape. *Immunol. Rev.* **2008**, *222*, 206–221.
- (4) Prendergast, G. C. Immune escape as a fundamental trait of cancer: focus on IDO. *Oncogene* **2008**, *27*, 3889–3900.
- (5) Yamamoto, S.; Hayaishi, O. Tryptophan pyrrolase of rabbit intestine. D- and L-tryptophan-cleaving enzyme or enzymes. *J. Biol. Chem.* **1967**, *242*, 5260–5266.

(6) Sono, M.; Roach, M.; Coulter, E.; Dawson, J. Heme-Containing Oxygenases. *Chem. Rev.* **1996**, *96*, 2841–2888.

(7) Munn, D. H.; Zhou, M.; Attwood, J. T.; Bondarev, I.; Conway, S. J.; Marshall, B.; Brown, C.; Mellor, A. L. Prevention of allogeneic fetal rejection by tryptophan catabolism. *Science* **1998**, *281*, 1191–1193.

(8) Hwu, P.; Du, M. X.; Lapointe, R.; Do, M.; Taylor, M. W.; Young, H. A. Indoleamine 2,3-dioxygenase production by human dendritic cells results in the inhibition of T cell proliferation. *J. Immunol.* **2000**, *164*, 3596–3599.

(9) Terness, P.; Bauer, T. M.; Röse, L.; Dufter, C.; Watzlik, A.; Simon, H.; Opelz, G. Inhibition of allogeneic T cell proliferation by indoleamine 2,3-dioxygenase-expressing dendritic cells: mediation of suppression by tryptophan metabolites. *J. Exp. Med.* **2002**, *196*, 447–457.

(10) Fallarino, F.; Grohmann, U.; You, S.; McGrath, B. C.; Cavener, D. R.; Vacca, C.; Orabona, C.; Bianchi, R.; Belladonna, M. L.; Volpi, C.; Santamaria, P.; Fioretti, M. C.; Puccetti, P. The combined effects of tryptophan starvation and tryptophan catabolites down-regulate T cell receptor zeta-chain and induce a regulatory phenotype in naive T cells. *J. Immunol.* **2006**, *176*, 6752–6761.

(11) Uyttenhove, C.; Pilotte, L.; Théate, I.; Stroobant, V.; Colau, D.; Parmentier, N.; Boon, T.; Van den Eynde, B. J. Evidence for a tumoral immune resistance mechanism based on tryptophan degradation by indoleamine 2,3-dioxygenase. *Nature Med.* **2003**, *9*, 1269–1274.

(12) Godin-Ethier, J.; Hanafi, L.-A.; Piccirillo, C. A.; Lapointe, R. Indoleamine 2,3-dioxygenase expression in human cancers: clinical and immunologic perspectives. *Clin. Cancer Res.* **2011**, *17*, 6985–6991.

(13) Muller, A. J.; DuHadaway, J. B.; Donover, P. S.; Sutanto-Ward, E.; Prendergast, G. C. Inhibition of indoleamine 2,3-dioxygenase, an immunoregulatory target of the cancer suppression gene Bin1, potentiates cancer chemotherapy. *Nature Med.* **2005**, *11*, 312–319.

(14) Ou, X.; Cai, S.; Liu, P.; Zeng, J.; He, Y.; Wu, X.; Du, J. Enhancement of dendritic cell-tumor fusion vaccine potency by indoleamine-pyrrole 2,3-dioxygenase inhibitor, 1-MT. *J. Cancer Res. Clin. Oncol.* **2008**, *134*, 525–533.

(15) Liu, X.; et al. Selective inhibition of IDO1 effectively regulates mediators of antitumor immunity. *Blood* **2010**, *115*, 3520–3530.

(16) Ino, K. Indoleamine 2,3-dioxygenase and immune tolerance in ovarian cancer. *Curr. Opin. Obstet. Gynecol.* **2011**, *23*, 13–18.

(17) Opitz, C. A.; et al. An endogenous tumour-promoting ligand of the human aryl hydrocarbon receptor. *Nature* **2011**, *478*, 197–203.

(18) Pilotte, L.; Larrieu, P.; Stroobant, V.; Colau, D.; Dolusic, E.; Frédérick, R.; Plaen, E. D.; Uyttenhove, C.; Wouters, J.; Masereel, B.; den Eynde, B. J. V. Reversal of tumoral immune resistance by inhibition of tryptophan 2,3-dioxygenase. *Proc. Natl. Acad. Sci. U.S.A.* **2012**, *109*, 2497–2502.

(19) Metz, R.; Duhadaway, J. B.; Kamasani, U.; Laury-Kleintop, L.; Muller, A. J.; Prendergast, G. C. Novel tryptophan catabolic enzyme IDO2 is the preferred biochemical target of the antitumor indoleamine 2,3-dioxygenase inhibitory compound D-1-methyl-tryptophan. *Cancer Res.* **2007**, *67*, 7082–7087.

(20) Ball, H. J.; Sanchez-Perez, A.; Weiser, S.; Austin, C. J. D.; Astelbauer, F.; Miu, J.; McQuillan, J. A.; Stocker, R.; Jermini, L. S.; Hunt, N. H. Characterization of an indoleamine 2,3-dioxygenase-like protein found in humans and mice. *Gene* **2007**, *396*, 203–213.

(21) Witkiewicz, A. K.; Costantino, C. L.; Metz, R.; Muller, A. J.; Prendergast, G. C.; Yeo, C. J.; Brody, J. R. Genotyping and expression analysis of IDO2 in human pancreatic cancer: a novel, active target. *J. Am. Coll. Surg.* **2009**, *208*, 781–787.

(22) Yuasa, H. J.; Ball, H. J.; Austin, C. J. D.; Hunt, N. H. 1-L-Methyltryptophan is a more effective inhibitor of vertebrate IDO2 enzymes than 1-D-methyltryptophan. *Comp. Biochem. Physiol., Part B: Biochem. Mol. Biol.* **2010**, *157*, 10–15.

(23) Meininger, D.; Zalameda, L.; Liu, Y.; Stepan, L. P.; Borges, L.; McCarter, J. D.; Sutherland, C. L. Purification and kinetic characterization of human indoleamine 2,3-dioxygenases 1 and 2 (IDO1 and IDO2) and discovery of selective IDO1 inhibitors. *Biochim. Biophys. Acta* **2011**, *1814*, 1947–1954.

- (24) Wogulis, M.; Chew, E. R.; Donohoue, P. D.; Wilson, D. K. Identification of formyl kynurenine formamidase and kynurenine aminotransferase from *Saccharomyces cerevisiae* using crystallographic, bioinformatic and biochemical evidence. *Biochemistry* **2008**, *47*, 1608–1621.
- (25) Sugimoto, H.; Oda, S.; Otsuki, T.; Hino, T.; Yoshida, T.; Shiro, Y. Crystal structure of human indoleamine 2,3-dioxygenase: catalytic mechanism of O<sub>2</sub> incorporation by a heme-containing dioxygenase. *Proc. Natl. Acad. Sci. U.S.A.* **2006**, *103*, 2611–2616.
- (26) Chauhan, N.; Basran, J.; Efimov, I.; Svistunenko, D. A.; Seward, H. E.; Moody, P. C. E.; Raven, E. L. The role of serine 167 in human indoleamine 2,3-dioxygenase: a comparison with tryptophan 2,3-dioxygenase. *Biochemistry* **2008**, *47*, 4761–4769.
- (27) Efimov, I.; Basran, J.; Thackray, S. J.; Handa, S.; Mowat, C. G.; Raven, E. L. Structure and reaction mechanism in the heme dioxygenases. *Biochemistry* **2011**, *50*, 2717–2724.
- (28) Vottero, E.; Mitchell, D. A.; Page, M. J.; MacGillivray, R. T. A.; Sadowski, I. J.; Roberge, M.; Mauk, A. G. Cytochrome b(5) is a major reductant in vivo of human indoleamine 2,3-dioxygenase expressed in yeast. *FEBS Lett.* **2006**, *580*, 2265–2268.
- (29) Maghzal, G. J.; Thomas, S. R.; Hunt, N. H.; Stocker, R. Cytochrome b<sub>5</sub>, not superoxide anion radical, is a major reductant of indoleamine 2,3-dioxygenase in human cells. *J. Biol. Chem.* **2008**, *283*, 12014–12025.
- (30) Pearson, J. T.; Siu, S.; Meininger, D. P.; Wienkers, L. C.; Rock, D. A. In vitro modulation of cytochrome P450 reductase supported indoleamine 2,3-dioxygenase activity by allosteric effectors cytochrome b(5) and methylene blue. *Biochemistry* **2010**, *49*, 2647–2656.
- (31) Watanabe, Y.; Fujiwara, M.; Hayaishi, O. 2,5-Dihydro-L-phenylalanine: a competitive inhibitor of indoleamine 2,3-dioxygenase. *Biochem. Biophys. Res. Commun.* **1978**, *85*, 273–279.
- (32) Sono, M.; Cady, S. G. Enzyme kinetic and spectroscopic studies of inhibitor and effector interactions with indoleamine 2,3-dioxygenase. I. Norharman and 4-phenylimidazole binding to the enzyme as inhibitors and heme ligands. *Biochemistry* **1989**, *28*, 5392–5399.
- (33) Cady, S. G.; Sono, M. 1-Methyl-DL-tryptophan, beta-(3-benzofuranyl)-DL-alanine (the oxygen analog of tryptophan), and beta-[3-benzo(b)thienyl]-DL-alanine (the sulfur analog of tryptophan) are competitive inhibitors for indoleamine 2,3-dioxygenase. *Arch. Biochem. Biophys.* **1991**, *291*, 326–333.
- (34) Peterson, A. C.; Loggia, A. J. L.; Hamaker, L. K.; Arend, R. A.; Fisette, P. L.; Okazi, Y.; Will, J. A.; Brown, R. R.; Cook, J. M. Evaluation of Substituted  $\beta$ -Carbolines as Noncompetitive Indoleamine 2,3-Dioxygenase Inhibitors. *Med. Chem. Res.* **1993**, *3*, 473–482.
- (35) Peterson, A. C.; Migawa, M. T.; Martin, M. J.; Hamaker, L. K.; Czerwinski, K. M.; Zhang, W.; Arend, R. A.; Fisette, P. L.; Okazi, Y.; Will, J. A.; Brown, R. R.; Cook, J. M. Evaluation of Functionalized Tryptophan Derivatives and Related Compounds as Competitive Inhibitors of Indoleamine 2,3-Dioxygenase. *Med. Chem. Res.* **1994**, *3*, 531–544.
- (36) Gaspari, P.; Banerjee, T.; Malachowski, W. P.; Muller, A. J.; Prendergast, G. C.; DuHadaway, J.; Bennett, S.; Donovan, A. M. Structure-activity study of brassinin derivatives as indoleamine 2,3-dioxygenase inhibitors. *J. Med. Chem.* **2006**, *49*, 684–692.
- (37) Brastianos, H. C.; Vottero, E.; Patrick, B. O.; Soest, R. V.; Matainaho, T.; Mauk, A. G.; Andersen, R. J.; Exiguamine, A an indoleamine-2,3-dioxygenase (IDO) inhibitor isolated from the marine sponge *Neopetrosia exigua*. *J. Am. Chem. Soc.* **2006**, *128*, 16046–16047.
- (38) Andersen, R.; Pereira, A.; Huang, X.-H.; Mauk, G.; Vottero, E.; Roberge, M.; Balgi, A. Indoleamine 2,3-Dioxygenase (IDO) Inhibitors. Patent WO 2006/005185, 2006.
- (39) Pereira, A.; Vottero, E.; Roberge, M.; Mauk, A. G.; Andersen, R. J. Indoleamine 2,3-dioxygenase inhibitors from the Northeastern Pacific Marine Hydroid *Garveia annulata*. *J. Nat. Prod.* **2006**, *69*, 1496–1499.
- (40) Andersen, R.; Leblanc, M.; Brastianos, H.; Vottero, E.; Roberge, M.; Mauk, G.; Carr, G. Substituted Quinone Indoleamine 2,3-Dioxygenase (IDO) Inhibitors and Synthesis and Uses Thereof. Patent WO 2008/052352, 2008.
- (41) Carr, G.; Chung, M. K. W.; Mauk, A. G.; Andersen, R. J. Synthesis of indoleamine 2,3-dioxygenase inhibitory analogues of the sponge alkaloid exiguamine A. *J. Med. Chem.* **2008**, *51*, 2634–2637.
- (42) Kumar, S.; Malachowski, W.; Duhadaway, J.; Lalonde, J.; Carroll, P.; Jaller, D.; Metz, R.; Prendergast, G.; Muller, A. Indoleamine 2,3-Dioxygenase Is the Anticancer Target for a Novel Series of Potent Naphthoquinone-Based Inhibitors. *J. Med. Chem.* **2008**, *51*, 1706–1718.
- (43) Carr, G.; Tay, W.; Bottrill, H.; Andersen, S. K.; Mauk, A. G.; Andersen, R. J. Plectosphaeric acids A, B, and C, indoleamine 2,3-dioxygenase inhibitors produced in culture by a marine isolate of the fungus *Plectosphaerella cucumerina*. *Org. Lett.* **2009**, *11*, 2996–2999.
- (44) Terentis, A. C.; Freewan, M.; Plaza, T. S. S.; Raftery, M. J.; Stocker, R.; Thomas, S. R. The selenazal drug ebselen potently inhibits indoleamine 2,3-dioxygenase by targeting enzyme cysteine residues. *Biochemistry* **2010**, *49*, 591–600.
- (45) Vottero, E.; Balgi, A.; Woods, K.; Tugendreich, S.; Melese, T.; Andersen, R. J.; Mauk, A. G.; Roberge, M. Inhibitors of human indoleamine 2,3-dioxygenase identified with a target-based screen in yeast. *Biotechnol. J.* **2006**, *1*, 282–288.
- (46) Kumar, S.; Jaller, D.; Patel, B.; LaLonde, J. M.; DuHadaway, J. B.; Malachowski, W. P.; Prendergast, G. C.; Muller, A. J. Structure based development of phenylimidazole-derived inhibitors of indoleamine 2,3-dioxygenase. *J. Med. Chem.* **2008**, *51*, 4968–4977.
- (47) Dolušić, E.; et al. Indol-2-yl ethanones as novel indoleamine 2,3-dioxygenase (IDO) inhibitors. *Bioorg. Med. Chem.* **2011**, *19*, 1550–1561.
- (48) Dolušić, E.; et al. Discovery and preliminary SARs of keto-indoles as novel indoleamine 2,3-dioxygenase (IDO) inhibitors. *Eur. J. Med. Chem.* **2011**, *46*, 3058–3065.
- (49) Matsuno, K.; Takai, K.; Isaka, Y.; Unno, Y.; Sato, M.; Takikawa, O.; Asai, A. S-Benzylisothiourea derivatives as small-molecule inhibitors of indoleamine-2,3-dioxygenase. *Bioorg. Med. Chem. Lett.* **2010**, *20*, 5126–5129.
- (50) Smith, J. R.; Evans, K. J.; Wright, A.; Willows, R. D.; Jamie, J. F.; Griffith, R. Novel indoleamine 2,3-dioxygenase-1 inhibitors from a multistep in silico screen. *Bioorg. Med. Chem.* **2012**, *20*, 1354–1363.
- (51) Yue, E. W.; et al. Discovery of potent competitive inhibitors of indoleamine 2,3-dioxygenase with in vivo pharmacodynamic activity and efficacy in a mouse melanoma model. *J. Med. Chem.* **2009**, *52*, 7364–7367.
- (52) Koblisch, H. K.; Hansbury, M. J.; Bowman, K. J.; Yang, G.; Neilan, C. L.; Haley, P. J.; Burn, T. C.; Waeltz, P.; Sparks, R. B.; Yue, E. W.; Combs, A. P.; Scherle, P. A.; Vaddi, K.; Fridman, J. S. Hydroxyamidine inhibitors of indoleamine-2,3-dioxygenase potently suppress systemic tryptophan catabolism and the growth of IDO-expressing tumors. *Mol. Cancer Ther.* **2010**, *9*, 489–498.
- (53) Röhrig, U. F.; Awad, L.; Grosdidier, A.; Larrieu, P.; Stroobant, V.; Colau, D.; Cerundolo, V.; Simpson, A. J. G.; Vogel, P.; Van den Eynde, B. J. V.; Zoete, V.; Michielin, O. Rational design of indoleamine 2,3-dioxygenase inhibitors. *J. Med. Chem.* **2010**, *53*, 1172–1189.
- (54) Huang, Q.; Zheng, M.; Yang, S.; Kuang, C.; Yu, C.; Yang, Q. Structure-activity relationship and enzyme kinetic studies on 4-aryl-1H-1,2,3-triazoles as indoleamine 2,3-dioxygenase (IDO) inhibitors. *Eur. J. Med. Chem.* **2011**, *46*, 5680–5687.
- (55) Grosdidier, A.; Zoete, V.; Michielin, O. EADock: docking of small molecules into protein active sites with a multiobjective evolutionary optimization. *Proteins* **2007**, *67*, 1010–1025.
- (56) Grosdidier, A.; Zoete, V.; Michielin, O. Blind docking of 260 protein-ligand complexes with EADock 2.0. *J. Comput. Chem.* **2009**, *30*, 2021–2030.
- (57) Grosdidier, A.; Zoete, V.; Michielin, O. SwissDock, a protein-small molecule docking web service based on EADock DSS. *Nucleic Acids Res.* **2011**, *39*, W270–W277.
- (58) Grosdidier, A.; Zoete, V.; Michielin, O. Fast docking using the CHARMM force field with EADock DSS. *J. Comput. Chem.* **2011**, *32*, 2149–2159.

- (59) Zoete, V.; Grosdidier, A.; Cuendet, M.; Michielin, O. Use of the FACTS solvation model for protein–ligand docking calculations. Application to EADock. *J. Mol. Recognit.* **2010**, *23*, 457–461.
- (60) Zoete, V.; Cuendet, M. A.; Grosdidier, A.; Michielin, O. SwissParam: a fast force field generation tool for small organic molecules. *J. Comput. Chem.* **2011**, *32*, 2359–2368.
- (61) Röhrig, U. F.; Grosdidier, A.; Zoete, V.; Michielin, O. Docking to Heme Proteins. *J. Comput. Chem.* **2009**, *30*, 2305–2315.
- (62) Kallander, L. S.; et al. 4-Aryl-1,2,3-triazole: a novel template for a reversible methionine aminopeptidase 2 inhibitor, optimized to inhibit angiogenesis in vivo. *J. Med. Chem.* **2005**, *48*, 5644–5647.
- (63) Oh, S.; Shin, W.-S.; Ham, J.; Lee, S. Acid-catalyzed synthesis of 10-substituted triazolyl artemisinins and their growth inhibitory activity against various cancer cells. *Bioorg. Med. Chem. Lett.* **2010**, *20*, 4112–4115.
- (64) Agalave, S. G.; Maujan, S. R.; Pore, V. S. Click chemistry: 1,2,3-triazoles as pharmacophores. *Chem. Asian J.* **2011**, *6*, 2696–2718.
- (65) Siddiquia, N.; Ahsana, W.; Alama, M. S.; Alia, R.; Jainb, S.; Azada, B.; Akhtara, J. Trizaoles: as potential bioactive agents. *Int. J. Pharm. Sci. Rev. Res.* **2011**, *8*, 161–169.
- (66) Gubbins, P. O. Triazole antifungal agents drug–drug interactions involving hepatic cytochrome P450. *Expert Opin. Drug Metab. Toxicol.* **2011**, *7*, 1411–1429.
- (67) Kolb, H. C.; Finn, M. G.; Sharpless, K. B. Click Chemistry: Diverse Chemical Function from a Few Good Reactions. *Angew. Chem., Int. Ed. Engl.* **2001**, *40*, 2004–2021.
- (68) Tornøe, C. W.; Christensen, C.; Meldal, M. Peptidotriazoles on solid phase: [1,2,3]-triazoles by regioselective copper(I)-catalyzed 1,3-dipolar cycloadditions of terminal alkynes to azides. *J. Org. Chem.* **2002**, *67*, 3057–3064.
- (69) Rostovtsev, V. V.; Green, L. G.; Fokin, V. V.; Sharpless, K. B. A stepwise Huisgen cycloaddition process: copper(I)-catalyzed regioselective “ligation” of azides and terminal alkynes. *Angew. Chem., Int. Ed. Engl.* **2002**, *41*, 2596–2599.
- (70) Zoete, V.; Grosdidier, A.; Schuepbach, T.; Michielin, O. manuscript in preparation.
- (71) Jin, T.; Kamijo, S.; Yamamoto, Y. Copper-Catalyzed Synthesis of *N*-Unsubstituted 1,2,3-Triazoles from Nonactivated Terminal Alkynes. *Eur. J. Org. Chem.* **2004**, *18*, 3789–3791.
- (72) Arcadi, A.; Cacchi, S.; Del Rosario, M.; Fabrizi, G.; Marinelli, F. Palladium-Catalyzed Reaction of *o*-Ethylnylphenols, *o*-((Trimethylsilyl)ethynyl)phenyl Acetates, and *o*-Alkynylphenols with Unsaturated Triflates or Halides: A Route to 2-Substituted-, 2,3-Disubstituted-, and 2-Substituted-3-acylbenzo[b]furans. *J. Org. Chem.* **1996**, *61*, 9280–9288.
- (73) Han, G.; Tamaki, M.; Hruby, V. J. Fast, efficient and selective deprotection of the *tert*-butoxycarbonyl (Boc) group using HCl/dioxane (4 m). *J. Pept. Res.* **2001**, *58*, 338–341.
- (74) Tóth, G.; Kövér, K. E. Simple, Safe, Large Scale Synthesis of 5-Arylmethyl-2,2-dimethyl-1,3-dioxane-4,6-diones and 3-Arylpropanoic Acids. *Synth. Commun.* **1995**, *25*, 3067–3074.
- (75) Pak, J.; Hesse, M. Regioselective Deprotection and Acylation of Penta-*N*-Protected Thermopentamine. *Helv. Chim. Acta* **1998**, *81*, 2300–2313.
- (76) Kawai, N.; Shiori, T. New Methods and Reagents in Organic Synthesis. 34. Diphenyl Phosphorazidate (DPPA) as a 1,3-Dipole. A Simple, Efficient Conversion of Alkyl Phenyl Ketones to 2-Phenyl-alkanoic Acids. *Chem. Pharm. Bull.* **1983**, *31*, 2564–2573.
- (77) Jiang, Y.; Kuang, C.; Yang, Q. The Use of Calcium Carbide in the Synthesis of 1-Monosubstituted Aryl 1,2,3-Triazole. *Synlett* **2009**, 2009, 3163–3166.
- (78) Li, P.; Wang, L. One-Pot Synthesis of 1,2,3-Triazoles from Benzyl and Alkyl Halides, Sodium Azide and Alkynes in Water Under Transition-Metal-Catalyst Free Reaction Conditions. *Lett. Org. Chem.* **2007**, *4*, 23–26.
- (79) George, S. R. D.; Edwards, G. L.; Harper, J. B. The effects of ionic liquids on azide–alkyne cycloaddition reactions. *Org. Biomol. Chem.* **2010**, *8*, 5354–5358.
- (80) Liu, D.; Gao, W.; Dai, Q.; Zhang, X. Triazole-based monophosphines for Suzuki–Miyaura coupling and amination reactions of aryl chlorides. *Org. Lett.* **2005**, *7*, 4907–4910.
- (81) Kadaba, P. K. Triazolines. 14. 1,2,3-Triazolines and triazoles, a new class of anticonvulsants. Drug design and structure–activity relationships. *J. Med. Chem.* **1988**, *31*, 196–203.
- (82) Jiang, X.; Tiwari, A.; Thompson, M.; Chen, Z.; Cleary, T. P.; Lee, T. B. K. A Practical Method for *N*-Methylation of Indoles Using Dimethyl Carbonate. *Org. Process Res. Dev.* **2001**, *5*, 604–608.
- (83) Kozima, S.; Itano, T.; Mihara, N.; Sisido, K.; Isida, T. Formation of organotin–nitrogen bonds IV. *N*-Trialkyltin derivatives of 4-mono- or 4,5-disubstituted 1,2,3-triazoles, 3-phenyl-1,2,4-triazole, 3-phenyl-pyrazole and 4-phenylimidazole. *J. Organomet. Chem.* **1972**, *44*, 117–126.
- (84) Butler, R. N. A Study of the Proton Nuclear Magnetic Resonance Spectra of Aryl and Mono- and Disubstituted *N*-Methylazoles. *Can. J. Chem.* **1973**, *51*, 2315–2322.
- (85) Bénétteau, V.; Olmos, A.; Boningari, T.; Sommer, J.; Pale, P. Zeo-click synthesis: CuI-zeolite-catalyzed one-pot two-step synthesis of triazoles from halides and related compounds. *Tetrahedron Lett.* **2010**, *51*, 3673–3677.
- (86) Wang, X.-J.; Sidhu, K.; Zhang, L.; Campbell, S.; Haddad, N.; Reeves, D. C.; Krishnamurthy, D.; Senanayake, C. H. Bromo-directed *N*-2 alkylation of *NH*-1,2,3-triazoles: efficient synthesis of poly-substituted 1,2,3-triazoles. *Org. Lett.* **2009**, *11*, 5490–5493.
- (87) Eguchi, N.; Watanabe, Y.; Kawanishi, K.; Hashimoto, Y.; Hayaishi, O. Inhibition of indoleamine 2,3-dioxygenase and tryptophan 2,3-dioxygenase by beta-carboline and indole derivatives. *Arch. Biochem. Biophys.* **1984**, *232*, 602–609.
- (88) Lu, C.; Lin, Y.; Yeh, S.-R. Spectroscopic studies of ligand and substrate binding to human indoleamine 2,3-dioxygenase. *Biochemistry* **2010**, *49*, 5028–5034.
- (89) Schofield, K.; Grimmett, M. R.; Keene, B. R. T. *Heteroaromatic Nitrogen Compounds: The Azoles*; Cambridge University Press: New York, 1976.
- (90) Hansch, C.; Leo, A. *Substituent Constants for Correlation Analysis in Chemistry and Biology*; Wiley: New York, 1979.
- (91) Sono, M.; Andersson, L. A.; Dawson, J. H. Sulfur donor ligand binding to ferric cytochrome P-450-CAM and myoglobin. Ultraviolet–visible absorption, magnetic circular dichroism, and electron paramagnetic resonance spectroscopic investigation of the complexes. *J. Biol. Chem.* **1982**, *257*, 8308–8320.
- (92) Tomasi, J.; Mennucci, B.; Cammi, R. Quantum mechanical continuum solvation models. *Chem. Rev.* **2005**, *105*, 2999–3093.
- (93) Brooks, B. R.; Bruccoleri, R. E.; Olafson, B. D.; States, D. J.; Swaminathan, S.; Karplus, M. CHARMM: A Program for Macromolecular Energy, Minimization, and Dynamics Calculations. *J. Comput. Chem.* **1983**, *4*, 187–217.
- (94) MacKerell, A. D., Jr.; et al. All-Atom Empirical Potential for Molecular Modeling and Dynamics Studies of Proteins. *J. Phys. Chem. B* **1998**, *102*, 3586–3616.
- (95) Haberthür, U.; Caflisch, A. FACTS: Fast analytical continuum treatment of solvation. *J. Comput. Chem.* **2008**, *29*, 701–715.
- (96) Hopkins, A. L.; Groom, C. R.; Alex, A. Ligand efficiency: a useful metric for lead selection. *Drug Discovery Today* **2004**, *9*, 430–431.
- (97) Austin, C. J. D.; Astelbauer, F.; Kosim-Satyaputra, P.; Ball, H. J.; Willows, R. D.; Jamie, J. F.; Hunt, N. H. Mouse and human indoleamine 2,3-dioxygenase display some distinct biochemical and structural properties. *Amino Acids* **2009**, *36*, 99–106.
- (98) Miranker, A.; Karplus, M. Functionality maps of binding sites: a multiple copy simultaneous search method. *Proteins* **1991**, *11*, 29–34.
- (99) Adamo, C.; Barone, V. Toward reliable density functional methods without adjustable parameters: The PBE0 model. *J. Chem. Phys.* **1999**, *110*, 6158–6169.
- (100) Frisch, M. J. et al. *Gaussian 09*, revision A.1; Gaussian Inc.: Wallingford, CT, 2009.

- (101) Schaefer, A.; Huber, C.; Ahlrichs, R. Fully optimized contracted Gaussian-basis sets of triple zeta valence quality for atoms Li to Kr. *J. Chem. Phys.* **1994**, *100*, 5829–5835.
- (102) Reed, A. E.; Weinstock, R. B.; Weinhold, F. Natural-population analysis. *J. Chem. Phys.* **1985**, *83*, 735–746.
- (103) Dunning, T. H., Jr. Gaussian basis sets for use in correlated molecular calculations. I. The atoms boron through neon and hydrogen. *J. Chem. Phys.* **1989**, *90*, 1007–1023.
- (104) Kendall, R. A.; Dunning, T. H., Jr.; Harrison, R. J. Electron affinities of the first-row atoms revisited. Systematic basis sets and wave functions. *J. Chem. Phys.* **1992**, *96*, 6796–6806.
- (105) Woon, D. E.; Dunning, T. H., Jr. Gaussian-basis sets for use in correlated molecular calculations. 3. The atoms aluminum through argon. *J. Chem. Phys.* **1993**, *98*, 1358–1371.
- (106) Martin, F.; Zipse, H. Charge distribution in the water molecule—a comparison of methods. *J. Comput. Chem.* **2005**, *26*, 97–105.
- (107) Cheng, Y.; Prusoff, W. H. Relationship between the inhibition constant (K<sub>i</sub>) and the concentration of inhibitor which causes 50% inhibition (I<sub>50</sub>) of an enzymatic reaction. *Biochem. Pharmacol.* **1973**, *22*, 3099–3108.
- (108) Cer, R. Z.; Mudunuri, U.; Stephens, R.; Lebeda, F. J. IC<sub>50</sub>-to-K<sub>i</sub>: a web-based tool for converting IC<sub>50</sub> to K<sub>i</sub> values for inhibitors of enzyme activity and ligand binding. *Nucleic Acids Res.* **2009**, *37*, W441–W445.
- (109) Koumbis, A. E.; Kyzas, C. M.; Savva, A.; Varvoglis, A. Formation of new alkynyl(phenyl)iodonium salts and their use in the synthesis of phenylsulfonyl indenes and acetylenes. *Molecules* **2005**, *10*, 1340–1350.
- (110) Kempson, J.; et al. Synthesis, initial SAR and biological evaluation of 1,6-dihydroimidazo[4,5-*d*]pyrrolo[2,3-*b*]pyridin-4-amine derived inhibitors of IkkapB kinase. *Bioorg. Med. Chem. Lett.* **2009**, *19*, 2646–2649.
- (111) Malamas, M. S.; Robichaud, A. J.; Porte, A. M.; Morris, K. M.; Solvibile, W. R.; Kim, J.-i. Amino-5-[4-(difluoromethoxy)phenyl]-5-phenylimidazolone Compounds for the Inhibition of  $\beta$ -Secretase. Patent WO/2008/118379, 2008.
- (112) Fischer, C.; Methot, J.; Zhou, H.; Schell, A. J.; Munoz, B.; Rivkin, A. A.; Ahearn, S. P.; Chichetti, S.; MacCoss, R. N.; Kattar, S. D.; Christopher, M.; Li, C.; Rosenau, A.; Brown, W. C. Triazole Derivatives For Treatment of Alzheimer's Disease. Patent WO/2010/071741, 2010.
- (113) Conte, A.; Kuehne, H.; Luebbbers, T.; Mattei, P.; Maugeais, C.; Mueller, W.; Pflieger, P. Anthranilamide/2-amino-heteroarene Carboxamide Derivatives. Patent WO/2007/090752, 2007.
- (114) Carroll, W. A.; Kalvin, D. M.; Medrano, A. P.; Florjancic, A. S.; Wang, Y.; Donnelly-Roberts, D. L.; Namovic, M. T.; Grayson, G.; Honoré, P.; Jarvis, M. F. Novel and potent 3-(2,3-dichlorophenyl)-4-(benzyl)-4*H*-1,2,4-triazole P2X<sub>7</sub> antagonists. *Bioorg. Med. Chem. Lett.* **2007**, *17*, 4044–4048.
- (115) Musso, D. L.; Clarke, M. J.; Kelley, J. L.; Boswell, G. E.; Chen, G. Novel 3-phenylprop-2-ynylamines as inhibitors of mammalian squalene epoxidase. *Org. Biomol. Chem.* **2003**, *1*, 498–506.
- (116) Yoo, E. J.; Chang, S. A new route to indolines by the Cu-catalyzed cyclization reaction of 2-ethynylanilines with sulfonyl azides. *Org. Lett.* **2008**, *10*, 1163–1166.
- (117) Park, J. H.; Bhilare, S. V.; Youn, S. W. NHC-catalyzed oxidative cyclization reactions of 2-alkynylbenzaldehydes under aerobic conditions: synthesis of O-heterocycles. *Org. Lett.* **2011**, *13*, 2228–2231.
- (118) Jones, C. D.; Luke, R. W. A.; McCoull, W. *Saminopyrimidine Derivates With TIE2 Inhibiting Activity*. Patent WO/2006/103449, 2006.
- (119) Yates, K.; Mandrapilas, G. Vinyl cation intermediates in solvolytic and electrophilic reactions. 2. Bromination of arylacetylenes. *J. Org. Chem.* **1980**, *45*, 3902–3906.
- (120) Cohrt, A. E.; Jensen, J. F.; Nielsen, T. E. Traceless azido linker for the solid-phase synthesis of *NH*-1,2,3-triazoles via Cu-catalyzed azide–alkyne cycloaddition reactions. *Org. Lett.* **2010**, *12*, 5414–5417.
- (121) Jiang, Y.; Kuang, C.; Yang, Q. Copper(I) Iodide-Catalyzed Synthesis of 4-Aryl-1*H*-1,2,3-triazoles from anti-3-Aryl-2,3-dibromopropanoic Acids and Sodium Azide. *Synthesis* **2010**, *2010*, 4256–4260.
- (122) Roppe, J.; Smith, N. D.; Huang, D.; Tehrani, L.; Wang, B.; Anderson, J.; Brodtkin, J.; Chung, J.; Jiang, X.; King, C.; Munoz, B.; Varney, M. A.; Prasit, P.; Cosford, N. D. P. Discovery of novel heteroarylazoles that are metabotropic glutamate subtype 5 receptor antagonists with anxiolytic activity. *J. Med. Chem.* **2004**, *47*, 4645–4648.
- (123) Lyga, J. W.; Zawacki, F.; Zhang, L. Y. *Phenylalkyl Substituted Heteroaryl Derivatives*. Patent WO/2006/130403, 2006.
- (124) Buckler, R. T.; Hartzler, H. E.; Kurchacova, E.; Nichols, G.; Phillips, B. M. Synthesis and antiinflammatory activity of some 1,2,3- and 1,2,4-triazolepropionic acids. *J. Med. Chem.* **1978**, *21*, 1254–1260.
- (125) Coelho, A.; Diz, P.; Caamaño, O.; Sotelo, E. Polymer-Supported 1,5,7-Triazabicyclo[4.4.0]dec-5-ene as Polyvalent Ligands in the Copper-Catalyzed Huisgen 1,3-Dipolar Cycloaddition. *Adv. Synth. Catal.* **2010**, *352*, 1179–1192.
- (126) Zhang, W.; Kuang, C.; Yang, Q. Palladium-Catalyzed One-Pot Synthesis of 4-Aryl-1*H*-1,2,3-triazoles from anti-3-Aryl-2,3-dibromopropanoic Acids and Sodium Azide. *Synthesis* **2010**, *2010*, 287–283.
- (127) Kallander, L. S.; Ryan, D. M.; Thompson, S. K. Compounds And Methods. Patent WO/2003/031434, 2003.
- (128) Makriyannis, A.; Pandarinathan, L.; Zvonok, N.; Parkkari, T.; Chapman, L. Inhibitors of fatty acid amide hydrolase and monoacylglycerol lipase for modulation of cannabinoid receptors. Patent WO/2009/117444, 2009.
- (129) Lu, L.-H.; Wu, J.-H.; Yang, C.-H. Preparation of 1*H*-1,2,3-triazoles by cuprous ion mediated cycloaddition of terminal alkyne and sodium azide. *J. Chinese Chem. Soc.* **2008**, *55*, 414–417.
- (130) Takikawa, O.; Kuroiwa, T.; Yamazaki, F.; Kido, R. Mechanism of interferon-gamma action. Characterization of indoleamine 2,3-dioxygenase in cultured human cells induced by interferon-gamma and evaluation of the enzyme-mediated tryptophan degradation in its anticellular activity. *J. Biol. Chem.* **1988**, *263*, 2041–2048.
- (131) Albert, A.; Serjeant, E. *The Determination of Ionization Constants*, 3rd ed.; Chapman and Hall: New York, 1984.
- (132) Pettersen, E. F.; Goddard, T.; Huang, C.; Couch, G.; Greenblatt, D.; Meng, E.; Ferrin, T. E. UCSF Chimera—A Visualization System for Exploratory Research and Analysis. *J. Comput. Chem.* **2004**, *25*, 1605–1612.
- (133) Trifonov, R.; Shcherbinin, M.; Ostrovskii, V. A. Behavior of 4-Phenyl-1,2,3-triazole in Media of Various Acidities. *Russ. J. Org. Chem.* **1997**, *33*, 1046–1047.
- (134) Abboud, J.-L. M.; Foces-Foces, C.; Notario, R.; Trifonov, R. E.; Volovodenco, A. P.; Ostrovskii, V. A.; Alkorta, I.; Elguero, J. Basicity of *N-H*- and *N-Methyl*-1,2,3-triazoles in the Gas Phase, in Solution, and in the Solid State—An Experimental and Theoretical Study. *Eur. J. Org. Chem.* **2001**, *2001*, 3013–3024.
- (135) *CRC Handbook of Chemistry and Physics*, 92nd ed.; Haynes, W. M., Ed.; CRC Press: Boca Raton, FL, 2011–2012.